

Antioxidants & Redox Signaling

Antioxidants & Redox Signaling: <http://mc.manuscriptcentral.com/liebert/ARS>

Mitochondrial complex I reversible S-nitrosation improves bioenergetics and is protective in Parkinson's disease

Journal:	<i>Antioxidants and Redox Signaling</i>
Manuscript ID	ARS-2017-6992.R3
Manuscript Type:	Original Research Communication
Date Submitted by the Author:	10-Aug-2017
Complete List of Authors:	Milanesi, Chiara; Erasmus Medical Center, Molecular Genetics; Ri.MED Foundation Tapias, Victor; University of Pittsburgh, Neurology Gabriels, Sylvia; Erasmus Medical Center, Molecular Genetics Cerri, Silvia; Center for Research in Neurodegenerative Diseases, C. Mondino National Neurological Institute Levandis, Giovanna; Center for Research in Neurodegenerative Diseases, C. Mondino National Neurological Institute Tresini, Maria; Erasmus Medical Center, Molecular Genetics Blandini, Fabio; Center for Research in Neurodegenerative Diseases, C. Mondino National Neurological Institute Shiva, Sruti; Univ of Pittsburgh, Greenamyre, J; University of Pittsburgh, Department of Neurology and Pittsburgh Institute for Neurodegenerative Diseases Gladwin, Mark; University of Pittsburgh, Vascular Medicine Institute, and Pulmonary, Allergy and Critical Care Medicine Mastroberardino, Pier; Erasmus Medical Center, Genetics; University of Pittsburgh, Neurology
Keyword:	Central Nervous System, Mitochondria, Neurodegeneration, Nitric Oxide, Thiol, Drug Development
Manuscript Keywords (Search Terms):	Mitochondrial Complex I, Neurodegenerative disorders, neuroprotection, nitrite, Parkinson's disease

SCHOLARONE™
Manuscripts

Original Research Communication**Mitochondrial complex I reversible S-nitrosation improves bioenergetics and is protective in Parkinson's disease**

Chiara Milanese^{1,2}, Victor Tapias Molina^{3,4}, Sylvia Gabriels¹, Silvia Cerri⁵, Giovanna Levandis⁵, Fabio Blandini⁵, Maria Tresini¹, Sruti Shiva^{6,7}, Timothy J. Greenamyre^{3,4}, Mark T. Gladwin^{8,9}, and Pier G. Mastroberardino¹.

Affiliations

¹Department of Molecular Genetics, Erasmus Medical Center, 3015 CN Rotterdam, Netherlands

²Ri.MED Foundation, 90133 Palermo, Italy

³Department of Neurology, University of Pittsburgh, 15261 Pittsburgh, PA, USA

⁴Pittsburgh Institute for Neurodegenerative Diseases, University of Pittsburgh, 15261 Pittsburgh, PA, USA

⁵Laboratory of Functional Neurochemistry, Center for Research in Neurodegenerative Diseases, C. Mondino National Neurological Institute, 27100 Pavia, Italy

⁶Vascular Medicine Institute, University of Pittsburgh, 15261 Pittsburgh, PA, USA

⁷Department of Pharmacology & Chemical Biology, University of Pittsburgh, 15261 Pittsburgh, PA, USA

⁸Pittsburgh Heart, Lung, Blood and Vascular Medicine Institute and ⁹Division of Pulmonary, Allergy and Critical Care Medicine, Department of Medicine, University of Pittsburgh, 15261 Pittsburgh, PA, USA

⁹Division of Pulmonary, Allergy and Critical Care Medicine, Department of Medicine, University of Pittsburgh, 15261 Pittsburgh, PA, USA

Abbreviated title

1
2
3 Neuroprotection in Parkinson's disease
4

5
6 **Corresponding authors**
7

8 **Pier G. Mastroberardino** (designated author for communication with the Editorial and
9

10 Production offices)

11 Erasmus MC, Department of Molecular Genetics; Wytemaweg 80, 3015 CN Rotterdam,
12

13 Netherlands
14

15 Phone: +31-10-7043206
16

17 Fax: +31 10 704 47 43
18

19 Email: p.g.mastroberardino@erasmusmc.nl
20
21
22
23

24
25 **Chiara Milanese**
26

27 Erasmus MC, Department of Molecular Genetics; Wytemaweg 80, 3015 CN Rotterdam,
28

29 Netherlands
30

31 Phone: +31-10-7043206
32

33 Fax: +31 10 704 47 43
34

35 Email: c.milanese@erasmusmc.nl
36
37

38 **Word count** (Excluding references and figure legends): **7000**
39

40 **Reference numbers: 74**
41

42 **Number of greyscale illustrations: 2** (Fig. 3, Fig. 5)
43

44 **Number of color illustrations: 4 (online only: Fig.1, Fig. 2, Fig. 4 and Fig. 6)**
45

46 **Manuscript keywords:** Mitochondrial Complex I; neurodegenerative disorders;
47

48 neuroprotection; nitrite; Parkinson's disease
49
50
51
52
53
54
55
56
57
58
59
60

Abstract

Aims. The present study was designed to explore the neuroprotective potential of inorganic nitrite as a new therapeutic avenue in Parkinson's disease (PD).

Results. Administration of inorganic nitrite ameliorates neuropathology in phylogenetically distinct animal models of PD. Beneficial effects are not confined to prophylactic treatment and occur also if nitrite is administered when the pathogenic cascade is already active. Mechanistically, the effect is mediated by both complex I S-nitrosation, which under nitrite administration is favored over formation of other forms of oxidation, and as well as down-stream activation of the antioxidant Nrf2 pathway. Nitrite also rescues respiratory reserve capacity and increased proton leakage in LRRK2 PD patients' dermal fibroblasts.

Innovation. The study proposes an unprecedented approach based on the administration of the nitrosonium donor nitrite to contrast complex I and redox anomalies in PD. Dysfunctional mitochondrial complex I propagates oxidative stress in PD and treatments mitigating this defect may therefore limit disease progression. Therapeutic complex I targeting has been successfully achieved in ischemia/reperfusion by using nitrosonium donors such as nitrite to reversibly modify its subunits and protect from oxidative damage after reperfusion. This evidence led to the innovative hypothesis that nitrite could exert protective effects also in pathological conditions where complex I dysfunction occurs in normoxia, such as in PD.

Conclusions. Overall, these results demonstrate that administration of inorganic nitrite improves mitochondrial function in PD and it therefore represents an amenable intervention to hamper disease progression.

Introduction

Parkinson's disease (PD) is the prototypical movement disorder and is characterized by a progressive deterioration of the dopaminergic (DA) nigrostriatal circuits. A small fraction of PD cases are familial and attributable to single monogenic mutations; the vast majority of the disease, however, is sporadic and its etiology includes complex interactions between genetic and environmental factors. PD is a disease of advancing age and clinical manifestations appear relatively late in life; tremors, bradykinesia, postural instability, and rigidity are PD pathognomonic signs and manifest when a large proportion (~50%) of DA neurons are lost (41). At present, no effective cure for PD is available and therapies are limited to palliation of symptoms. Conventional wisdom has it that treatments retarding neuronal loss and preventing development of large lesions would be of great benefit for patients because they would arrest symptomatic deterioration. In view of the complexity of PD pathogenesis, which perturbs multiple cellular pathways, simultaneous targeting of different processes would increase the chance of therapeutic success.

Defects in mitochondrial respiratory complex I and oxidative stress have been consistently associated with PD by laboratory, clinical, and epidemiological studies, and are mechanistically interconnected (8,68,69). Complex I inhibition, in fact, results in increased production of mitochondrial reactive oxygen species (ROS) (66), which in turn may attack complex I amino acid residues in a positive feedback loop to generate irreversible damage (56) that exacerbates deterioration. Complex I therefore represents a tractable target in PD.

Targeting of complex I for therapeutic purposes has been principally explored in hypoxic pathological conditions, such as cardiac ischemia/reperfusion injury (20,67). These approaches relied on nitric oxide (NO) mediated modification of complex I, which favors reversible over irreversible thiol oxidation and prevents its abrupt reactivation during reperfusion, limiting the burst in ROS intrinsically associated with re-oxygenation (20,67). This strategy is therefore

1
2
3 based on induction of preventive mild oxidation, emulates traditional pre-conditioning, and leads
4 to significant mitigation of infarct size.
5
6

7 Inorganic nitrite is a biological reservoir for NO, which is produced after nitrite reduction by
8 myoglobin, hemoglobin, neuroglobin and/or xanthine oxidoreductase (45,46). Nitrite has been
9 shown to restore NO signaling and confer protection in ischemia/reperfusion via complex I
10 reversible S-nitrosation in multiple independent studies and in several organs, including liver,
11 heart, and brain (45,60). NO depletion and derangement of NO-mediated signaling occurs also
12 during aging and under oxidative stress (45). Investigations of nitrite-induced protective effects
13 has shown that – even in normoxic conditions - nitrite increases tolerance to subsequent
14 ischemia/reperfusion with a mechanism that modulates mitochondrial physiology and activates
15 protein kinases (39). These findings suggest that nitrite deserves consideration also in the
16 treatment of other conditions, particularly those where complex I defects and oxidative stress
17 play prominent pathogenic roles. PD largely fulfills these criteria.
18
19
20
21
22
23
24
25
26
27
28
29
30

31 The present study interrogated the potential of nitrite in normoxic conditions, as a
32 neuroprotective agent in PD, in multiple and phylogenetically diverse animal models, from
33 zebrafish to rodents. We examined the underlying mechanisms in a cellular model of DA
34 degeneration and translated our findings to human cases by studying nitrite effects on primary
35 dermal fibroblasts from familial PD patients with LRRK2 mutations, which are the most common
36 variants associated with this disease (42). Collectively, our data show that nitrite slows PD
37 progression and therefore holds clinical potential as disease modifying agent.
38
39
40
41
42
43
44
45
46
47
48
49
50
51
52
53
54
55
56
57
58
59
60

Results

Nitrite administration is protective in multiple pre-clinical animal models of PD

In a preliminary investigation, the potential of nitrite administration in PD was assessed in the small vertebrate zebrafish, which is a well-described model of PD (11,12,30,50,57). Two days treatment of larvae with the DA toxin MPP⁺ - the active metabolite of the prototypical PD toxin MPTP - results in selective degeneration of ascending DA neurons in the *posterior tuberculum* (PT), the homologue structure of the SNpc in zebrafish (40,63,65) (Fig. 1B, 1C, 1F-G). Administration of MPP⁺ constitutes an appropriate experimental setting for preliminary investigation of the neuroprotective potential of nitrite because it inhibits mitochondrial complex I (61) and causes redox imbalance (59). Due to its distinctive sensitivity to MPP⁺, the Tupfel long fin (TL) zebrafish strain was selected for the study (13). To exclude direct pharmacological interaction between nitrite and MPP⁺, the former was removed from the medium before addition of the neurotoxin (Fig. 1A). DA toxicity was evaluated by counting neurons in the ventral diencephalic clusters and the associated behavioral anomalies by measuring spontaneous motor activity and swimming velocity. As expected, 1mM MPP⁺ treatment for two consecutive days, starting at 5 days post-fertilization (dpf), induced significant loss of DA neurons in the PT (Fig. 1C) paralleled by sharp decrease in locomotor activity (Fig. 1N-P). Four days pretreatment with nitrite dissolved in E3 medium, starting at 1 dpf, resulted in dose-dependent neuroprotection and improvement in locomotor activity (Fig. 1C, 1N-P).

We next sought evidence for nitrite neuroprotection rodents. As expected, nitrite administration induces transient S-nitrosation of proteins extracted from the ventral mesencephalic region containing the SNpc (supplementary figure 4). Initially, we focused on the chronic progressive rotenone rat PD model. Chronic administration of low-doses of rotenone results in systemic inhibition of complex I, which in turn recapitulates essential features of PD including selective degeneration of SNpc DA neurons, oxidative stress, alpha-synuclein pathology, and

1
2
3 gastrointestinal neuropathology (8,18,26,37,48). Indeed, nitrite administration in drinking water -
4
5 initiated 72 hours before the first rotenone injection and continued until the end of the treatment
6
7 (Fig. 2A) - preserved DA projections in the striatum (Fig. 2B, and 2D) and significantly reduced
8
9 loss of DA neurons in the SNpc, as demonstrated by unbiased stereological counts (Fig. 2C,
10
11 and 2E).

12
13
14 To further substantiate the neuroprotective potential of nitrite in PD, investigations were
15
16 extended to the 6-hydroxydopamine (6-OHDA) rat model, in which pathology is experimentally
17
18 induced by unilateral intrastriatal injection of this toxin. This leads to progressive nigrostriatal
19
20 degeneration (9), caused by oxidative stress and by inhibition of complex I dependent
21
22 mitochondrial respiration (34,35). Importantly, the 6-OHDA model has been used to screen
23
24 potential neuroprotectants and all the drugs currently used in clinical practice effectively
25
26 ameliorate motor symptoms in 6-OHDA treated rats, with the only exception of antimuscarinic
27
28 compounds (27). Initial experiments addressed the effects of acute administration of nitrite
29
30 (2mg/kg), which was injected in rats 24 hours and 1 hour before stereotaxic infusion of 6-OHDA
31
32 (Fig. 2F - *Top panel*). Treatment resulted in significant reduction of the DA lesion (Fig. 2G-I,
33
34 *acute*). Subsequent experiments evaluated the effects of chronic treatment, where nitrite was
35
36 administered for three weeks in drinking water (50mg/L), starting 7 days after 6-OHDA infusion
37
38 (Fig. 2F - *Lower panel*), when degeneration of the nigrostriatal pathways is already pronounced
39
40 (10). Nitrite administration also successfully mitigated DA degeneration in this experimental
41
42 setup (Fig. 2G-I, *chronic*).

43 44 45 46 47 *Nitrite effects in human PD*

48
49
50 We next explored whether the nitrite effects observed in PD pre-clinical models could be
51
52 translated to human pathobiology. We investigated mitochondrial function in dermal fibroblasts
53
54 obtained from biopsies of patients harboring LRRK2 mutations (Table 1) (3,7,23,47), and used a
55
56 Seahorse Extracellular Flux Analyzer to characterize the bioenergetics profile of these cells (Fig.
57
58
59
60

1
2
3 3A). Out of the three studied PD lines, only one (ND32976) exhibited reduced basal respiration
4
5 (Fig. 3B). However, rotenone-sensitive respiration reflecting complex I activity was decreased in
6
7 all PD samples (Fig. 3C), substantiating the central role of mitochondrial complex I defects also
8
9 in genetic PD (23). Respiratory reserve capacity, which modulates the response to stress-
10
11 induced pathology (36), was also decreased in all specimens (Fig. 3D). Pretreatment with nitrite
12
13 (48 hours) led to significant improvement in both rotenone-sensitive respiration and reserve
14
15 capacity (Fig. 3F, G) in two of the LRRK2 mutant lines, but had no effect on cell lines from
16
17 controls (Table 1). Additionally, nitrite pretreatment significantly decreased basal H⁺ leakage in
18
19 LRRK2 samples (Fig. 3E) - therefore improving mitochondrial efficiency - in agreement with
20
21 previous observations (43); interestingly, nitrite augmented H⁺ leakage in control cells.
22
23
24
25

26 *Effects of nitrite on MPP⁺ treated SH-SY5Y cells*

27
28 To determine the mechanisms of action of nitrite-mediated neuroprotection observed *in vivo*, we
29
30 performed experiments in the SH-SY5Y DA cell line, which is commonly used as an *in vitro*
31
32 model of PD (66).
33
34
35

36 *Mechanisms affecting cell survival and protein redox state*

37
38 Consistent with previous data (4,28,66), administration of MPP⁺ affected cell survival, which was
39
40 significantly ameliorated by nitrite (Fig. 4A-C). Treatment with nitrite alone did not induce cell
41
42 death and protection was completely abolished by the NO scavenger carboxy-PTIO, thus
43
44 confirming that the observed effect was mediated by nitrite-derived NO (Fig. 4B, C).
45
46

47 Nitrite induced an increase in protein S-nitrosation in MPP⁺ treated SH-SY5Y, consistent with
48
49 augmented nitrite-dependent S-nitrosation (Fig. 4D, E - compare lanes 2, 3, and 5 - and
50
51 supplementary figure 1), whilst MPP⁺ alone did not alter S-nitrothiol levels (Fig. 4D, E compare
52
53 lanes 1 and 2). In nitrite/MPP⁺ co-treated samples, administration of the NO scavenger carboxy-
54
55 PTIO abolished the observed increase in S-nitrosothiol formation (Fig. 4D-E, compare lanes 3,
56
57
58
59
60

1
2
3 4, 5, 6). Replacement of nitrite with the NO donor 3,3-Bis(aminoethyl)-1-hydroxy-2-oxo-1-
4 triazene (NOC-18), which ensures sustained NO release because of its long half-life (21), led to
5 comparable results and further confirmed the central role of NO in the observed effects (Fig. 4D-
6 E, compare lanes 7 and 8).

7
8
9
10
11 Next, we explored whether increased reversible S-nitrosation could protect cysteine-thiols from
12 higher oxidation states (i.e. sulfinic and sulfonic acids), which can cause functional anomalies in
13 proteins and also predispose them to aggregation (62). Protein sulfenic acid formation induced
14 by hydrogen peroxide was significantly lessened by nitrite pre-treatment (Fig. 4F, G), confirming
15 that nitrite treatment favors reversible over irreversible thiol modification in proteins.

16
17
18
19
20
21
22
23
24
25
26
27
28
29
30
31
32
33
34
35
36
37
38
39
40
41
42
43
44
45
46
47
48
49
50
51
52
53
54
55
56
57
58
59
60
Nitrite administration did not abolish production of mitochondrial superoxide (Fig. 4H), in
agreement with previous studies showing that mitochondrial ROS production is required for
nitrite-mediated cytoprotection under normoxic conditions (39).

Mitochondrial respiration and complex I thiol redox status in MPP⁺ treated SH-SY5Y

The SH-SY5Y cell line was also used to evaluate the effects of nitrite administration on the
recovery of mitochondrial respiration after transient MPP⁺ challenge (25). Four-hour exposure to
MPP⁺ significantly suppressed basal mitochondrial respiration, and toxin removal was not
sufficient to promote full recovery. Contrastingly, samples pre-treated with nitrite successfully
restored respiration to control levels (Fig. 5A).

Next, the redox equilibrium between S-nitrosated and reduced cysteines was examined in
immunocaptured complex I. Nitrite increased S-nitrosation without altering levels of reduced
cysteines (Fig. 5B, compare lanes 2 and 6). However, when nitrite was co-administered with
MPP⁺, S-nitrosation was paralleled by a marked increment in reduced cysteine-thiol levels (Fig.
5B, compare lanes 3 and 7) reflecting a more reduced state of complex I (Fig. 5B, lane 8).
Nitrite-mediated improved respiration in MPP⁺ treated cells is therefore associated with
reduction of the thiol/disulfide redox equilibrium in complex I.

1
2
3 To clarify the mechanisms responsible for nitrite-mediated cysteine reduction in MPP⁺ treated
4 cells, we investigated activation of the major antioxidant cellular pathway Nrf2. Upon augmented
5 oxidation levels - or in the presence of NO - the Nrf2 transcription factor dissociates from its
6 cytosolic partner Keap1, translocates to the nucleus, and promotes transcription of several
7 genes involved in the antioxidant response (1,16,17,24,72). Nitrite pre-treatment in MPP⁺
8 challenged samples - which displayed reduced cysteines in complex I (Fig. 5B) – induced SNO
9 modification in Keap1 (Fig. 5C, D, and supplementary figure 2). Nitrite administration also
10 induced Nrf2 activation in SHSY-5Y cells overexpressing GFP-tagged Nrf2 (Fig. 6A-D). Nitrite
11 also induced nuclear translocation of endogenous Nrf2, as evidenced by immunochemical
12 detection in untransfected SHSY-5Y cells. Activation was also detected under physiological
13 conditions system S-nitrosation of Keap1, as expected, elicited nuclear Nrf2 translocation (Fig.
14 6E and supplementary figure 3). Collectively, these convergent data demonstrate nuclear
15 translocation of Nrf2, which was paralleled by increased expression of known target genes (Fig.
16 6H, I) therefore unambiguously establishing that nitrite causes activation of the Nrf2 pathway.
17 Activation of Nrf2 target genes was prevented, as expected, by the specific Nrf2 inhibitor
18 trigonelline (Fig. 6G). Nrf2 nuclear translocation depended upon nitrite-derived NO, as it was
19 markedly reduced by the NO scavenger carboxy-PTIO (Fig. 6F). Nrf2 activation was not
20 detectable in cells treated with MPP⁺ alone (Fig. 6B, D, E), consistently with the unaltered levels
21 of reduced cysteines in these samples (Fig. 5B).
22
23
24
25
26
27
28
29
30
31
32
33
34
35
36
37
38
39
40
41
42
43
44
45
46
47
48
49
50
51
52
53
54
55
56
57
58
59
60

Discussion

This study shows that administration of nitrite – a reservoir of bioavailable NO - is neuroprotective in several preclinical models of PD and ameliorates mitochondrial efficiency in dermal fibroblasts from PD patients. Nitrite reduces dopaminergic neuron loss in multiple models of PD and amelioration is not confined to prophylactic treatment. In fact, it is also observed when treatment is initiated at more advanced pathogenic stages, as evidenced in 6-OHDA rats treated one week after induction of the lesion. Nitrite treatment also corrects defective maximal respiratory capacity and increased proton leakage in LRRK2 mutant patients.

Our findings extend previous evidence in hypoxic settings demonstrating that nitrite is protective against ROS and complex I dysfunction (67) to normoxic conditions. Overall, the work emphasizes the role of NO signaling for proper biological function and confirms that reconstituting reserves of bioavailable NO preserves its integrity and protects against pathology (45). Importantly, reduced NO bioavailability characterizes conditions such as aging and oxidative stress, which constitute major risk factors for PD (22,45,69).

Our data are consistent with the notion that reactive species are essential signaling molecules – with effects that extend beyond mere toxicity and are instead essential for proper physiological function (5) - and are in agreement with evidence showing that NO exerts dichotomous effects depending on its concentration (45). Physiological NO levels ensure correct function and a moderate increase in NO may induce mild levels of stress, protecting against subsequent and more pronounced insults in a preconditioning-like manner (20). Consistently, we show that nitrite administration favors formation in complex I of S-nitrosothiols over sulfenic acid. Because the latter can be converted in higher and irreversible oxidation states (62), it is tempting to speculate that nitrite-induced S-nitrosation constitutes a molecular shield protecting cysteine

1
2
3 residues against permanent damage *in vivo*. Further studies to test this hypothesis are
4
5 warranted. Restoration of physiological NO levels can also scavenge superoxide to prevent an
6
7 escalation of oxidative stress (45). Conversely, high NO levels are toxic – in fact boosting NO
8
9 production via iNOS is part of the innate immune response to kill invading pathogens – and are
10
11 associated with neurodegeneration (52,64). The key success factor is therefore restoration of
12
13 NO bioavailability in a timely manner, before nitrosative/oxidative stress escalation.
14
15

16
17
18
19 While nitrosative stress has previously been reported in PD (19), there is no evidence that
20
21 exposure to NO releasing drugs is causative or even constitutes a risk factor for this disorder. In
22
23 fact, nitrosonium donors have been extensively used in clinical practice to treat cardiovascular
24
25 diseases and membrane permeable NO diffuses three-dimensionally from the cell of origin
26
27 therefore conceivably reaching neurons (31,51). Nonetheless, the use of this class of molecules
28
29 is not associated with increased PD prevalence. Conversely, a recent and intriguing study
30
31 highlighted an association between discontinuation of statin therapy and PD (44). Because
32
33 improvement of NO bioavailability – also at the cerebral level (32) - is a well described effect of
34
35 lipophilic statins, it is tempting to speculate that decreased NO levels following therapy
36
37 discontinuation might be detrimental for individuals at risk for PD.
38
39
40
41
42
43

44
45 Additionally, our results demonstrating that nitrite restores mitochondrial reserve capacity and
46
47 reduces proton leak in patients are consistent with similar, previous findings in healthy human
48
49 subjects showing that nitrite improves mitochondrial bioenergetics (43).
50
51
52
53

54
55 Mechanistically, we demonstrate that, in normoxia, nitrite acts along two parallel and likely
56
57 synergistic pathways involving complex I and Nrf2 activation. These findings are consistent with
58
59
60

1
2
3 previous evidence showing that NO is an activator of the Nrf2 pathway (53) with a mechanism
4 involving S-nitrosation of its cytosolic partner Keap1 (1,16,17,24,72). Additionally, it has been
5 recently demonstrated that, in normoxia, nitrite activates protein kinases (39), which in turn can
6 activate Nrf2 (55). Overall, our findings are consistent with the notion that nitrite is a complex
7 NO donor acting at multiple levels (33) and substantiate its therapeutic relevance given the
8 attention Nrf2 received as a target for neuroprotection (38). Future studies will be crucial in
9 identifying the signaling cascades leading to nitrite-mediated Nrf2 activation and to determine
10 whether other mitochondrial NO donors (e.g. mito-SNO (20)) retain the ability to activate Nrf2.

11
12 Nitrite is a source of bioavailable NO that has been successfully used in laboratory models of
13 cardiovascular diseases and is currently being scrutinized in clinical studies (45). Additionally,
14 currently available data support the safety of nitrite use in human therapeutics. Traditionally,
15 nitrite has been associated with two principal health related issues: methemoglobinemia - i.e.
16 nitrite-mediated oxidation of ferrous iron in hemoglobin to the ferric state - and an alleged
17 carcinogenic potential. None of these issues, however, constitute a threat under the
18 pharmacological conditions envisaged for human therapeutics. In fact, nitrite EC₅₀ to induce
19 methemoglobinemia is approximately 1gram (54), while the amount used in our and other
20 studies (46) is in the order of milligrams. Under these conditions, methemoglobinemia can be
21 safely excluded. Conversely, there is no evidence in favor of carcinogenic activity of nitrite, as
22 demonstrated by toxicological studies prolonging administration to two years periods (54) and
23 by epidemiological investigations as well (49). In summary, nitrite pharmacokinetics, safety, and
24 dosing features are known, and the molecule is therefore an excellent candidate for testing in
25 human PD.
26
27
28
29
30
31
32
33
34
35
36
37
38
39
40
41
42
43
44
45
46
47
48
49
50
51
52
53
54
55
56
57
58
59
60

1
2
3
4
5
6
7
8
9
10
11
12
13
14
15
16
17
18
19
20
21
22
23
24
25
26
27
28
29
30
31
32
33
34
35
36
37
38
39
40
41
42
43
44
45
46
47
48
49
50
51
52
53
54
55
56
57
58
59
60

Collectively, our study demonstrates that inorganic nitrite mitigates PD pathology through a synergistic mechanism improving mitochondrial efficiency and activating the Nrf2 antioxidant pathway, and therefore represents promising therapy for PD.

CONFIDENTIAL - For Peer Review Only

Innovation

Parkinson's disease is a neurodegenerative disorder significantly affecting quality of life. Strategies to cure it, or even to slow down its progression, are not available and therapies are limited to symptoms' palliation.

We demonstrate that administration of inorganic nitrite mitigates neuropathology in multiple PD models. Mechanistically, nitrite improves mitochondrial function and activates endogenous antioxidant defenses. Nitrite also corrects impaired mitochondrial bioenergetics in patients' fibroblasts.

Our study indicates that nitrite holds clinical potential as a novel therapeutic agent for PD. Nitrite is currently tested in clinical studies to treat cardiovascular conditions and it could therefore be easily repositioned for PD treatment.

Materials and Methods

Chemicals

Sodium Nitrite (563218), MPP⁺ (D048), MPTP (1-Methyl-4-phenyl-1,2,3,6-tetrahydropyridine hydrochloride, M0896), Carboxy-PTIO potassium salt (NO-scavenger, C221), 3,3-Bis(aminoethyl)-1-hydroxy-2-oxo-1-triazene (NO-donor, A5581), 6-hydroxydopamine hydrobromide (6-OHDA, H4381); oligomycin (75351); FCCP (C2920); rotenone (557368) and antimycin (A8674), N-Ethylmaleimide (NEM, E3876), digitonin (D141), mannitol (M4125), glutamate (1446600), malate (4694U), trigonelline (T5509), 5,5-Dimethyl-1,3-cyclohexanedione (dimedone, D153303) were obtained from Sigma-Aldrich (St. Louis, MO, USA).

Zebrafish treatment

Adult Tupfel long fin (TL) zebrafish were maintained at 28°C on a 14/10 hours light/dark cycles. Embryos were collected from natural mating and rose in E3 buffer (5mM NaCl, 0.17 mM KCl, 0.33 mM CaCl₂, 0.33 mM MgSO₄) at 28°C.

1day post fertilization zebrafish embryos (20 embryos/plate) were treated for 4 days with sodium nitrite (0.1-10 μM) dissolved in E3 buffer and incubated at 28°C. At day 5 fish were transferred to fresh E3 buffer and treated for 2 consecutive days with MPP⁺ 1 mM as previously described (29). The solutions were daily changed. At 7dpf zebrafish larvae were collected for behavioral testing or sacrificed to perform morphological analysis. Experiments were performed in accordance with the European Communities Council Directives (2010/63/EEC; D.L., 27.01.1992, number 116), the Dutch welfare legislation, and according to the guidelines of the Erasmus MC animal facility (EDC).

Zebrafish motor analysis

1
2
3 Larval motor activity was analyzed using the *Zebrolab* system (ViewPoint Life Sciences,
4 Montreal, Quebec, Canada) as previously described (50). Viewpoint software was used in
5 “tracking mode” with inactive/active and small/large thresholds respectively set to 0.5 and 1
6 mm/sec. Zebrafish larvae were analyzed in a 96 well plate containing 300 μ L of E3 buffer per
7 well in a single larva/well setup. Spontaneous activity was measured at 7dpf for hours, after 15
8 minutes of adaptation time following the transfer to the new *Zebrabox* setup.
9
10
11
12
13
14
15
16

17 *Zebrafish whole-mount immunohistochemistry*

18
19
20 Whole mount immunohistochemistry was carried out as previously described (50). All incubation
21 steps and washes were carried out on a shaker. Briefly, specimens were fixed in 4% PFA (from
22 PFA 16% - 28908, Thermo Fisher, Waltham, MA, USA)- 4% sucrose phosphate buffer saline
23 solution (PBS – 100110023, Thermo Fisher, Waltham, MA, USA) over night (ON) at 4°C. The
24 day after, larvae were washed in PBS ON at 4°C. After washes, eyes and yolk sack were
25 mechanically removed to improve antibody penetration in the brain tissue. Specimens were
26 permeabilized with Proteinase K (PK – P2308, Sigma-Aldrich) 10 μ g/mL for 15 minutes at room
27 temperature (RT) and washed 3 time 30 min with PBS containing 0.3% Tryton X-100 (PBS-T).
28 Larvae were then post-fixed in 4% PFA in PBS-T for 20 min at RT and then washed 3 times for
29 10 min with PBS-T at RT. Zebrafish were then blocked ON at 4°C in a solution containing
30 DMSO 1% and normal goat serum (NGS) 4% in PBS-T. Mouse monoclonal anti-tyrosine
31 hydroxylase (TH, 1:500; MAB318, Millipore, Billerica, MA, USA) incubation was performed ON
32 at 4°C in blocking buffer. Samples were washed 5 times for 30 min at RT with PBS-T and then
33 incubated with Alexa 488 anti-mouse secondary antibody (A32723, Thermo Fisher, Waltham,
34 MA, USA) ON at 4°C. After 5 washes in PBS-T, larvae transferred to an 80% glycerol solution
35 and mounted for confocal analysis. Image acquisition was performed in an inverted Leica TCS
36 SP5 confocal microscope (Leica Microsystems, Buffalo Grove, IL, USA) in a z-stack mode and
37
38
39
40
41
42
43
44
45
46
47
48
49
50
51
52
53
54
55
56
57
58
59
60

1
2
3 the cell counting in the *posterior tuberculum* (PT) area was performed analyzing all the
4 consecutive layers of the stack using the ImageJ software.
5
6
7

8 9 *Rotenone rat model*

10
11 Male Lewis rats were treated with rotenone as previously described (18). Briefly, animals were
12 treated up to 45 days (instead of 30). The first 30 days rats received an i.p. rotenone dose of 3
13 mg/kg/day and then, the dosage was increased to 3.5 mg/kg/day. Nitrite was administered in
14 drinking water, 1.5 g/L, for three consecutive days before starting the rotenone treatment. Six-
15 seven-month-old male Lewis rats were used for all experiments (Hilltop Lab Animals, Inc,
16 Scottsdale, PA, USA). The animals were maintained under standard conditions of temperature
17 and humidity, in 12 hours light/dark cycle, with free access to water and food. The rats were
18 adapted for 2 weeks prior to initiation of the experimental protocol. All studies were approved by
19 the Institutional Animal Care and Use Committee at the University of Pittsburgh and were
20 performed in accordance with published National Institutes of Health guidelines.
21
22
23
24
25
26
27
28
29
30
31
32

33 34 *6-OHDA rat model*

35
36 For the 6-OHDA model, male Sprague–Dawley rats (Charles River, Calco, LC, Italy) weighing
37 275–300 g were maintained under standard conditions of temperature and humidity with free
38 access to food and water at the Centralized Animal Facility of the University of Pavia.
39 Experiments were performed in accordance with the European Communities Council Directives
40 (2010/63/EEC; D.L., 27.01.1992, number 116) and the guidelines for animal experimentation
41 approved by the Animal Care Committees of the University of Pavia, Italy.
42
43
44
45
46
47
48

49 Animals were anesthetized by i.p. administration of 50 mg/kg of sodium-thiopental and placed in
50 a stereotaxic frame (Stoelting, Wood Dale, IL). They received an injection of 6-OHDA 20 mg per
51 3ml in saline containing 0.02% ascorbic acid) into the right striatum (1.0 mm anterior, 3.0 mm
52
53
54
55
56
57
58
59
60

1
2
3 lateral, and 5.0 mm ventral with respect to bregma and dura) at 1 ml/min, using a Hamilton 10-
4
5 AL syringe with a 26-gauge needle.

6
7 Twenty weeks old Sprague–Dawley rats subjected to the acute treatment were i.p.-injected with
8
9 2mg/kg of sodium nitrite in PBS 24 hours and 1 hour before 6-OHDA injection. Animals
10
11 underwent chronic treatment according to a previously reported administration paradigm (15),
12
13 and received nitrite orally, dissolved in drinking water (concentration: 50mg/L), for three weeks
14
15 starting 7 days after induction of the lesion.
16
17

18 19 *Cell cultures*

20
21 Skin dermal fibroblasts derived from PD patients bearing the G2019S (ND33879) or the
22
23 N1441G (ND32975 and ND32976) LRRK2 mutations and age matched controls were obtained
24
25 from the Coriell biorepository of the Coriell Institute for Medical Research (Camden, NJ, USA); a
26
27 detailed description is reported in Table 1. SH-SY5Y cells were obtained from Sigma-Aldrich
28
29 (94030304, St. Louis, MO, USA). Cells were cultured according to standard procedures at 37°C
30
31 and 5% CO₂ in DMEM medium (D6429, Sigma-Aldrich) supplemented with 10% of fetal bovine
32
33 serum (FBS – F6178, Sigma-Aldrich) and 1% penicillin-streptomycin (P4333, Sigma-Aldrich).
34
35 SH-SY5Y human neuroblastoma cell lines and PD-derived skin dermal fibroblast cell lines were
36
37 plated and after 24 hours treated for 2 consecutive days with sodium nitrite (1 or 10 μM)
38
39 dissolved in culture medium or vehicle. For SH-SY5Y cells, on the third day the nitrite-containing
40
41 medium was removed and fresh new media containing MPP⁺ 100 μM or vehicle was added to
42
43 the culture for 4 hours. After of incubation, cells were collected for analysis.
44
45
46
47
48

49 50 *Immunohistochemistry*

51
52 Immunohistological sections were processed as previously described (37). Briefly, sections
53
54 were first incubated in hydrogen peroxide (H₂O₂, Sigma-Aldrich, St. Louis, MO, USA) 3% in PBS
55
56 for 30 min to block internal peroxidases activity, and subsequently in PBS-Triton X-100 0.2%
57
58
59
60

1
2
3 (PBS-T) and normal horse serum (NHS) 10% for 1 hour at RT. Specimens were then incubated
4
5 for 24 h at 4°C with mouse monoclonal anti-Tyrosine hydroxylase (1:4000, MAB318, Millipore,
6
7 MA, USA), in PBS-T and 1.5% NHS. After several washes with PBS-T, sections were incubated
8
9 with biotinylated goat anti-rabbit IgG (1:500; BA 1000, Vector Laboratories, Burlingame, CA,
10
11 USA), in PBS and 1% NHS for 1 h at RT. Immuno-complexes were revealed by Vectastain Elite
12
13 ABC kit (PK 4000, Vector Laboratories, Burlingame, CA, USA), using 3,3'-diamino-benzidine
14
15 (DAB Substrate kit for Peroxidase, SK 4100, Vector Laboratories, Burlingame, CA, USA).
16
17 Finally, sections were dehydrated and mounted with Eukitt (Kindler GmbH & Co.). Slides were
18
19 observed with an Olympus BX 51(Olympus, Parkway Center Valley, PA, USA) microscope
20
21 equipped with a Leica DFC 420 camera.
22
23
24

25 26 *Quantification of striatal TH density*

27
28 Striatal lesion in DAB stained sections was calculated as the ratio between the lesioned area,
29
30 detected by the absence of TH staining, and the area of the entire TH immunopositive striatum
31
32 on the injected side (6). A total of 14 sections per animals were analyzed.
33
34

35
36 Alternatively, TH density was determined using an Odyssey infrared imaging system (LI-COR
37
38 Biosciences, Lincoln, NE, USA). Four to five serial immunofluorescence labeled sections were
39
40 scanned at 800 nm at high resolution to generate the reported average striatal DA fiber intensity
41
42 as previously described (70). The dorsal region of the striatum was outlined and the average
43
44 pixel intensity for each section was obtained using the Odyssey software (3.0).
45
46

47 *Unbiased stereological counts*

48
49 In rotenone treated rats, an automated Nikon 90i upright fluorescence microscope equipped
50
51 with five fluorescent channels and a linear encoded motorized stage was used to obtain a high
52
53 resolution montage for analysis as previously reported (71). SN images were collected at 20x
54
55 (0.75 N.A.) using a Q-imaging Retiga cooled CCD camera and the Nikon NIS-Elements
56
57
58
59
60

1
2
3 software (4.2). Unbiased quantification of TH-immunoreactive cells was assessed in the SN
4 pars compacta and reticulata from one hemisphere. All slides were scanned under the same
5 conditions for magnification, exposure time, lamp intensity, and camera gain. Following
6 background subtraction and thresholding, quantitative analysis was determined on fluorescent
7 images generated in three fluorescent colors (MAP2 in red; TH⁺ in green, and nuclei in blue) in
8 every sixth section throughout the entire region. An average of 11-12 sections per animal was
9 used for quantification. Stereological counts were coded and carried out by an experimenter
10 blinded to the treatment. The coefficient of error was calculated according to West & Gundersen
11 as above, and values were <0.10 in all cases.

12
13
14 In rats treated with 6-OHDA, unbiased stereological estimation of the total number of the
15 dopaminergic cells in SNpc was made using the optical fractionator method (West et al., 1991)
16 from the STEREO INVESTIGATOR program on a Neurolucida computer-controlled microscopy
17 system (Microbrightfield Inc., Williston, VT, USA). The edges of the SNc in the rostro-caudal
18 axis were defined at all levels, with reference to a coronal atlas of the mouse brain (58). TH-
19 positive cells in the SNc of both hemispheres were counted in every three section, on
20 comparable sections for all the subgroups of treatment throughout the entire nucleus. Counting
21 frames (60 x 60 μm) were placed at the intersections of a grid (frame size 120 x 120 μm) that
22 had been randomly placed over the section. Only counting frames for which at least a part of the
23 frame fell within the contour of the SNpc were used for counting. Cells were marked if they were
24 TH-positive and were in focus within the counting area. Guard volumes (3 μm from the top and
25 3 μm from the bottom of the section) were excluded from both surfaces to avoid the problem of
26 lost caps. The reliability of the estimate was assessed by calculation of the coefficient of error
27 according to the formulae described in West & Gundersen (74).

28 *Bioenergetic profiling*

1
2
3 The Seahorse XF24 Extracellular Flux Analyzer (Agilent Technologies, Santa Clara, Ca, USA)
4 was used to generate the bioenergetic profiles of human primary skin fibroblasts in real time and
5 neuroblastoma SH-SY5Y cell line as previously described (3). PD-LRRK2-derived fibroblasts
6 and healthy controls were seeded on a Seahorse XF-24 plate at a density of 6×10^4 cells per
7 well and grown overnight in DMEM (10% of FCS and 1% Pen-Strep) at 37°C in presence of
8 CO_2 . The density ensures a proportional response of FCCP with cell number (3) and resulted in
9 confluent cultures, in which cell growth was blocked by contact inhibition. After adhesion, cells
10 were then treated for 48 hours with sodium nitrite (1 or 10 μM) or vehicle (PBS) dissolved in
11 growth medium. Media were refreshed daily. On the experimental day, cells medium was
12 changed to unbuffered DMEM (XF Assay Medium – Agilent Technologies, Santa Clara, Ca,
13 USA) supplemented with 5 mM glucose and 1 mM sodium pyruvate, and incubated 1 hour at
14 37°C in absence of CO_2 . Medium and reagents were adjusted to pH 7.4 on the day of the
15 assay. After four baseline measurements for the oxygen consumption ratio (OCR), cells were
16 sequentially challenged with injections of mitochondrial toxins: 0.5 μM oligomycin (ATP
17 synthase inhibitor), 1 μM FCCP (mitochondrial respiration uncoupler), 0.5 μM rotenone
18 (complex I inhibitor), and 0.5 μM antimycin (complex III inhibitor).
19

20
21 SH-SY5Y cells were seeded at a density of 5×10^4 cells per well and let to adhere overnight. On
22 the next day, cells were treated for 48 hours with sodium nitrite or vehicle at the same
23 conditions as previously described for fibroblast lines. Culture medium was then removed and
24 cells were treated with MPP^+ 100 μM or vehicle (PBS) for 4 hours at 37°C . Medium was then
25 changed to unbuffered DMEM supplemented with 5mM glucose and 1 mM sodium pyruvate as
26 described and rested for 1 hour at 37°C without CO_2 . The recovery of mitochondrial respiration
27 was detected for 8 hours (25), followed three measurements after the injection of 1 μM FCCP,
28 used to test cell viability at the end of the assay.
29

30
31
32
33
34
35
36
37
38
39
40
41
42
43
44
45
46
47
48
49
50
51
52
53
54
55
56
57
58
59
60
Detection of protein sulfenic acid production after H_2O_2 treatment in cultured cells

1
2
3 Confluent SH-SY5Y cells were shortly treated (10 and 30 seconds) with 0.5 mM H₂O₂ dissolved
4 in serum free medium and immediately suspended in RIPA buffer containing dimedone (NaCl
5 150 mM, NP-40 1%, DOC 0.1%, SDS 0.1%, Tris-HCl 50 mM, Dimedone 1 mM and protease
6 inhibitors) (2). After 45 minutes of incubation in ice, protein samples were processed, separated
7 on a NuPAGE precast SDS PAGE gel (NP0321, Thermo Fisher, Waltham, MA, USA) under
8 reducing conditions and transferred on a PVDF membrane. The membrane was blocked for 1
9 hour at RT in a PBS-T solution containing BSA 5% and proteins were detected through the
10 cysteine (sulfonate) polyclonal antibody (1:1000, ON at 4° C; ADI-OSA-820-F, ENZO,
11 Farmingdale, NY, USA) and the goat anti-Rabbit HRP-conjugated secondary antibody (1:5000;
12 P0487; DAKO-Agilent Technologies Santa Clara, CA, USA). The signal was then revealed with
13 the ECL detection system (GE Healthcare, Barrington, IL, USA). After detection, the membrane
14 was washed several times with PBS-T and incubated with the anti-actin mouse primary antibody
15 (1:4000, ON at 4° C; MAB 1501; Chemicon, Temecula, CA, USA) and the IRDye donkey-anti-
16 mouse secondary antibody (1:5000; Li-COR Biosciences, Lincoln, NE, USA). The signal was
17 finally detected using the Odyssey Imaging System (Li-COR Biosciences, Lincoln, NE, USA).
18
19
20
21
22
23
24
25
26
27
28
29
30
31
32
33
34
35

36 *SH-SY5Y cytotoxicity assays and superoxide production*

37
38
39 To investigate cellular toxicity in SH-SY5Y, cells were treated with nitrite dissolved in culture
40 medium at the described concentration. After 48 hours, the solution was replaced with fresh
41 medium containing MPP⁺. Cellular necrosis was evaluated after 24 hours of treatment with
42 MPP⁺ with Sytox green 0.5 μM (Invitrogen, Carlsbad, CA, USA), following manufacturer's
43 instructions, using a flow cytometer (FACSaria, BD Biosciences, San Jose CA, USA). FlowJo
44 Software (Tree Star Inc., Ashland, OR, USA) was used for data analysis. Cellular cytotoxicity
45 was further confirmed via lactate dehydrogenase release (LDH colorimetric detection kit,
46 630117, Cloneteck, Mountain View, CA, USA). Briefly 6×10⁴ cells were seeded in a 96 well
47 plate and treated with nitrite dissolved in DMEM (without phenol red, 21063029, Thermo Fisher,
48
49
50
51
52
53
54
55
56
57
58
59
60

1
2
3 Waltham, MA, USA) for 48 hours and then exposed to MPP⁺. After 24 hours, culture medium
4
5 was collected after centrifugation and then checked for lactate dehydrogenase content following
6
7 manufacturer's guidelines.
8

9
10 Mitochondrial superoxide production was detected using Mitosox Red (M36008, Invitrogen,
11
12 Carlsbad, CA, USA) following the manufacturer's guidelines. Briefly, after 4 hours exposure to
13
14 MPP⁺, 10⁶ cells were harvested and quickly washed in ice cold HBSS without Ca⁺⁺ and Mg⁺⁺,
15
16 and resuspended in Hepes 0.1 M containing Mitosox 0.2 μM. Cells were incubated 20 minutes
17
18 at 37° C, protected from light, and then analyzed with a FACSAria flow cytometer (BD
19
20 Biosciences, San Jose CA, USA).
21

22 23 24 *Detection of S-nitrosation levels in proteins*

25
26 S-nitrosated proteins were detected as previously described, with minor modifications (73).
27
28 Briefly, equal amount of cells (5×10⁵) were harvested via trypsin digestion and suspended in a
29
30 lysis solution containing Tris-HCl 50 mM, SDS 1%, NEM 100 mM and proteinase inhibitors mix
31
32 (Complete mini, 11836153001, ROCHE, Indianapolis, IN, USA). Lysates were incubated 5
33
34 minutes at 70° C, sonicated 15 minutes in cold-water bath and then incubated 30 minutes at
35
36 room temperature. Protein extracts were then precipitated with a cold solution of acetone,
37
38 methanol, ethanol (50%, 25%, and 25% respectively) suspended in the staining solution
39
40 containing Tris-HCl 50 mM, SDS 1%, 20 μM fluorescent Alexa-NEM-800 dye (929-80020, LI-
41
42 COR Biosciences, Lincoln, NE, USA) or EZ-Link PEG₂-Biotin NEM (21901BID, Thermo Fisher,
43
44 Waltham, MA, USA), ascorbate 1 mM and CuCl₂ 1μM, and incubated 1 hour at room
45
46 temperature. The staining solution was removed following acetone-methanol-ethanol
47
48 precipitation and proteins were finally suspended in Tris-HCl 50 mM, SDS 1% and Alexa Fluor
49
50 680 succinimidyl ester (NHS – A20008, Thermo Fisher, Waltham, MA, USA) 20μM. Samples
51
52 were diluted in Laemni Sample buffer containing 5% B-mercaptoethanol and proteins were
53
54 separated on a NuPAGE precast SDS PAGE gel (NP0321, Invitrogen, Carlsbad, CA, USA)
55
56
57
58
59
60

1
2
3 under reducing conditions. After electrophoresis, the gel was fixed with 50% ethanol 50% and
4 2.5% orthophosphoric acid overnight under mild agitation. Final images and analysis were
5 performed with the Odyssey Imaging System (Li-COR Biosciences, Lincoln, NE, USA).
6
7
8
9
10 Immunodetection of the mitochondrial protein Ndufa9 (1:1000, ab14713, Abcam, Cambridge,
11 MA, USA) in the extracts processed for the S-nitrosation assay was achieved by western blot
12 analysis performed according to standard procedures.
13
14
15
16

17 *Detection of SNO modification in Keap1*

18
19
20 SNO protein modifications were detected as described in the previous paragraph by using the
21 EZ-Link PEG₂-Biotin NEM during the staining step. Total S-nitrosylated proteins were isolated
22 via the Streptavidin Mag Separose kit (28-9872-30 AA, GE Healthcare, Aurora, WI, USA)
23 according manufacturer's protocol. Briefly, equal amount of biotin-SNO modified proteins were
24 incubated with 100 μ L of streptavidin magnetic beads ON at 4° C under slow end-over end
25 rotation. The biotin-streptavidin complex was then washed sequentially with: 1 - 0.2 M borate pH
26 9; 2 - 0.2M sodium acetate pH 4, and 3 - TBS-Urea buffer (50 mM Tris-HCl pH 7, 150 mM NaCl
27 and 2M Urea) and Biotin-SNO proteins were finally eluted in 100 μ L of elution buffer (Tris-HCl
28 50 mM, 150 mM NaCl, SDS 2%, 0.4% Urea) at 95 ° C for 10 minutes. Samples were then
29 treated with 4X Sample buffer and 25 μ L of the final solution was separated on the NuPAGE
30 precast SDS PAGE gel and transferred on a PVDF membrane. The membrane was blocked for
31 1 hour at RT in a PBS-T solution containing BSA 5% and SNO-biotinylated proteins were
32 detected for Keap1 (1:1000, ON at 4° C; 8046S, Cell Signaling, Danver, MA, USA) and the goat
33 anti-Rabbit HRP-conjugated secondary antibody (1:5000; P0487; DAKO-Agilent Technologies
34 Santa Clara, CA, USA). The signal was then revealed with the ECL detection system (GE
35 Healthcare, Barrington, IL, USA). As loading control, biotin-SNO samples were incubated with
36 20 μ M Alexa Fluor 680 succinimidyl ester and equal amounts were separated on a NuPAGE
37 precast SDS PAGE gel under reducing conditions. After electrophoresis, the gel was fixed with
38
39
40
41
42
43
44
45
46
47
48
49
50
51
52
53
54
55
56
57
58
59
60

1
2
3 50% ethanol 50% and 2.5% orthophosphoric acid ON under mild agitation. Final images and
4
5 analysis were performed with the Odyssey Imaging System (Li-COR Biosciences, Lincoln, NE,
6
7 USA).
8
9

10 *GFP-Nrf2 transient expression*

11
12
13 Transient expression of the pcDNA3-EGFP-C4-Nrf2 vector (21549, Addgene, Cambridge, MA,
14
15 USA) or the vector alone was achieved in SH-SY5Y cells by using X-tremeGENE HP DNA
16
17 transfection reagent (XTGHP-RO ROCHE, Sigma-Aldrich) according manufacturer's procedure.
18
19 24 hours after transfection cells were treated with nitrite/MPP⁺ as previously described and were
20
21 then collected for analysis. For IF analysis, cells were rinsed twice with PBS and then fixed 20'
22
23 with PFA 4%, rinsed 3 times with PBS, covered with Vectashield containing DAPI (H1200,
24
25 Vector laboratories Vector Laboratories, Burlingame, CA, USA) and then mounted on glass
26
27 slides. Image acquisition was performed in Zeiss LSM700 laser scanning confocal microscope.
28
29 Alternatively, cells were lysed in Tris-HCl 50 mM, SDS 1%, EDTA 1 mM, proteinase inhibitors
30
31 (Complete Mini). Lysates were separated on a NuPAGE precast SDS PAGE gel and
32
33 transferred on PVDF. The membrane was blocked for 1 hour at RT in a PBS-T solution
34
35 containing BSA 5% and GFP expressing proteins were detected with the anti-GFP antibody (1h
36
37 at RT; 1:1000. 11814460, Sigma-Aldrich) and the goat anti-mouse HRP-conjugated secondary
38
39 antibody (1:5000; 715-035-150; Jackson Immuno Research, West Grove, PA, USA). The signal
40
41 was then revealed with the ECL detection system (GE Healthcare, Barrington, IL, USA).
42
43
44
45

46 *Complex I immunoprecipitation and detection of thiol and S-nitrosothiols*

47
48
49 Mitochondria from SH-SY5Y neuroblastoma cells were isolated according to the "Mitochondria
50
51 Isolation Kit for Cultured Cells" guidelines (ab110171; Abcam, Cambridge, MA, USA), with
52
53 minor modifications. Briefly, 4×10⁸ confluent cells were collected by trypsin treatment and
54
55 suspended in mannitol 75 mM, sucrose 25 mM, KCl 100 μM, KH₂PO₄, MgCl₂ 5 mM, Tris-HCl 20
56
57
58
59
60

1
2
3 mM, glutamate 5 mM, malate 5 mM, digitonin 0.01%, NEM 10 mM and AlexaFluor maleimide-
4
5 800 20 μ M. Samples were processed 3 consecutive times with a homogenation step (Dounce
6
7 pestle “B”, 30 strokes) and mitochondria collection by centrifugation at 12000 g, 10 minutes at
8
9 4° C. Freshly isolated mitochondria were suspended in PBS, 10% maltoside, protease
10
11 inhibitors, NEM 10 mM and Alexa-NEM-800 dye (929-80020, LI-COR Biosciences, Lincoln, NE,
12
13 USA) 20 μ M at 5 mg/ml and mitochondrial complex I was immune-captured according to the
14
15 “Complex I immunocapture kit” guidelines (ab109711, Abcam, Cambridge, MA, USA). Isolated
16
17 complex I was further processed for S-nitrosation detection assay with the addition of
18
19 AlexaFluor-C2 Maleimide (NEM-680 dye – A20344, Thermo Fisher, Waltham, MA, USA) 20 μ M,
20
21 ascorbate 1 mM and CuCl 1 μ M to the solution and incubated 1 hour at room temperature.
22
23 Samples were finally diluted in Laemni Sample buffer containing 5% β -mercaptoethanol and
24
25 complex I proteins were separated on a NuPAGE precast SDS PAGE gel (NP0321, Invitrogen,
26
27 Carlsbad, CA, USA) under reducing conditions. After electrophoresis, the gel was fixed ethanol
28
29 in 50%, orto-phosphoric acid 2.5% ON under mild agitation. After image acquisition with an
30
31 Odyssey Imaging System (Li-COR Biosciences, Lincoln, NE, USA), the gel was finally
32
33 processed for silver staining, which was detected with a GS900 Calibrated Densitometer (Bio-
34
35 Rad, Irvine, CA, USA).

41 *Nrf2 mobilization and evaluation of antioxidant genes transcription*

42
43
44 Nrf2 activation was investigated in SH-SY5Y neuroblastoma cell line. 10^5 cells were seeded on
45
46 a glass coverslip, let adhere overnight, and treated as above with nitrite (48 hours) and/or MPP⁺
47
48 (4 hours). When required, NO-scavenger (Carboxy-PTIO) or the Nrf2 inhibitor trigonelline were
49
50 added to culture medium at the indicated concentration. Cells were then fixed and
51
52 permeabilized with PFA 4% and Triton 0.5% for 20 minutes at RT. Subsequently, cells were
53
54 blocked with BSA 3% in PBS for 1 hour at RT and incubated with the anti-Nrf2-antibody (1:100,
55
56 Sc-722, Santa Cruz, Ca, USA) in PBS supplemented with 1.5% BSA ON at 4° C. After 3
57
58
59
60

1
2
3 washes with PBS, cells were incubated 2 hours at RT with a fluorescent secondary antibody
4 (1:500, anti Rabbit Cy3 conjugated). Finally, coverslips were covered with Vectashield
5 (1:500, anti Rabbit Cy3 conjugated). Finally, coverslips were covered with Vectashield
6 containing DAPI (H1200, Vector laboratories Vector Laboratories, Burlingame, CA, USA) and
7 mounted on glass slides. Image acquisition was performed in a Leica TCS SP5 laser scanning
8 confocal microscope. Images were analyzed in a semi-automated fashion using the Metamorph
9 software (MolecularDevices, Sunnyvale, CA, USA). The software automatically quantified the
10 Nrf2 signal intensity generating regions of interest (ROI) around the nucleus based on the DAPI
11 fluorescence.

12
13
14
15
16
17
18
19
20
21
22
23
24
25
26
27
28
29
30
31
32
33
34
35
36
37
38
39
40
41
42
43
44
45
46
47
48
49
50
51
52
53
54
55
56
57
58
59
60

Total RNA was isolated from SH-SY5Y cells treated with nitrite and MPP⁺ as above. Total RNA was isolated using the RNAqueous Kit (AM1912, Ambion, Austin, TX, USA) according to manufactures directions. cDNA was synthesized with SuperScript First-Strand cDNA Synthesis Kit (11904018, Invitrogen, Carlsbad, CA, USA) from 1µg of RNA. qPCR was performed on a C1000TM Thermal Cycler, CFX96 Real-Time System (Bio-Rad, Irvine, CA, USA) using SYBR Green I (S7564, Invitrogen, Carlsbad, CA, USA) and Platinum Taq polymerase (10966018, Invitrogen, Carlsbad, CA, USA). Primer sequences were obtained from the PrimerBank PCR Primers database for Gene Expression Detection and Quantification (<http://pga.mgh.harvard.edu/primerbank>) and are described in Table 2. Data represent the average of values obtained from biological and experimental triplicates ± standard deviation. Expression was normalized against the average combined expression of two different housekeeping genes (Tyrosine 3-monooxygenase/tryptophan 5-monooxygenase activation protein zeta polypeptide -YWHAZ; and Homo sapiens ribosomal protein, large, P0 -RPLP0) (14).

Statistical analysis

All values are expressed as mean ± s.e.m. Statistical significance was assessed by two sided Student's t-test or one-way analysis of variance (ANOVA) followed by the Dunnett's multiple

1
2
3 comparison *post hoc* test. In all instances a value of $P < 0.05$ was considered as statistically
4
5 different.
6
7
8
9
10
11
12
13
14
15
16
17
18
19
20
21
22
23
24
25
26
27
28
29
30
31
32
33
34
35
36
37
38
39
40
41
42
43
44
45
46
47
48
49
50
51
52
53
54
55
56
57
58
59
60

Acknowledgments

The authors are grateful to Dr. Peter Holland for providing constructive criticism on the manuscript. *Fundings:* PGM was supported by a grant from the Netherlands Genomics Initiative (NGI/NWO 05040202), a Marie Curie grant (IRG 247918), and the CEREBRAD grant under the EU-FP7 framework (project number 295552). The Extracellular Flux Analyzer by Seahorse Bioscience was purchased thanks to a generous donation from the “Dorpman-Wigmans Stichting” (PGM). CM was supported by the Ri.MED Foundation.

Authors Disclosure Statement

The authors have declared that no conflict of interest exists.

List of Abbreviations

(6-OHDA) 6-hydroxydopamine; (DA) dopaminergic; (dpf) day post fertilization; (EDC) Erasmus MC animal facility; (NO) nitric oxide; (NOC-18) 3,3-Bis(aminoethyl)-1-hydroxy-2-oxo-1-triazene; (OCR) oxygen consumption rate; (ON) over night; (PD) Parkinson's disease; (PT) posterior tuberculum; (ROS) reactive oxygen species; (RT) room temperature; (SH) reduced cisteines; (SNO) S-nitrosated cisteines; (TH) Tyrosine Hydroxylase; (TL) Tupfel long fin.

References

1. Abbas K, Breton J, Planson AG, Bouton C, Bignon J, Seguin C, Riquier S, Toledano MB, Drapier JC. Nitric oxide activates an Nrf2/sulfiredoxin antioxidant pathway in macrophages. *Free Radic Biol Med* 51: 107-14, 2011.
2. Alvarez B, Carballal S, Turell L, Radi R. Formation and reactions of sulfenic acid in human serum albumin. *Methods Enzymol* 473: 117-36, 2010.
3. Ambrosi G, Ghezzi C, Sepe S, Milanese C, Payan-Gomez C, Bombardieri CR, Armentero MT, Zangaglia R, Pacchetti C, Mastroberardino PG, Blandini F. Bioenergetic and proteolytic defects in fibroblasts from patients with sporadic Parkinson's disease. *Biochim Biophys Acta* 1842: 1385-94, 2014.
4. Andoh T, Chock PB, Chiueh CC. The roles of thioredoxin in protection against oxidative stress-induced apoptosis in SH-SY5Y cells. *J Biol Chem* 277: 9655-60, 2002.
5. Angelova PR, Abramov AY. Functional role of mitochondrial reactive oxygen species in physiology. *Free Radic Biol Med* 100: 81-85, 2016.
6. Armentero MT, Fancellu R, Nappi G, Bramanti P, Blandini F. Prolonged blockade of NMDA or mGluR5 glutamate receptors reduces nigrostriatal degeneration while inducing selective metabolic changes in the basal ganglia circuitry in a rodent model of Parkinson's disease. *Neurobiol Dis* 22: 1-9, 2006.
7. Auburger G, Klinkenberg M, Drost J, Marcus K, Morales-Gordo B, Kunz WS, Brandt U, Broccoli V, Reichmann H, Gispert S, Jendrach M. Primary skin fibroblasts as a model of Parkinson's disease. *Mol Neurobiol* 46: 20-7, 2012.
8. Betarbet R, Sherer TB, MacKenzie G, Garcia-Osuna M, Panov AV, Greenamyre JT. Chronic systemic pesticide exposure reproduces features of Parkinson's disease. *Nat Neurosci* 3: 1301-6, 2000.
9. Blandini F, Armentero MT. Animal models of Parkinson's disease. *FEBS J* 279: 1156-66, 2012.
10. Blandini F, Levandis G, Bazzini E, Nappi G, Armentero MT. Time-course of nigrostriatal damage, basal ganglia metabolic changes and behavioural alterations following intrastriatal injection of 6-hydroxydopamine in the rat: new clues from an old model. *Eur J Neurosci* 25: 397-405, 2007.
11. Bortolotto JW, Cognato GP, Christoff RR, Roesler LN, Leite CE, Kist LW, Bogo MR, Vianna MR, Bonan CD. Long-term exposure to paraquat alters behavioral parameters and dopamine levels in adult zebrafish (*Danio rerio*). *Zebrafish* 11: 142-53, 2014.
12. Bretaud S, Lee S, Guo S. Sensitivity of zebrafish to environmental toxins implicated in Parkinson's disease. *Neurotoxicol Teratol* 26: 857-64, 2004.
13. Bretaud S, MacRaidl S, Ingham PW, Bandmann O. The influence of the zebrafish genetic background on Parkinson's disease-related aspects. *Zebrafish* 8: 103-8, 2011.
14. Bruce KD, Sihota KK, Byrne CD, Cagampang FR. The housekeeping gene YWHAZ remains stable in a model of developmentally primed non-alcoholic fatty liver disease. *Liver Int* 32: 1315-21, 2012.
15. Bryan NS, Calvert JW, Elrod JW, Gundewar S, Ji SY, Lefer DJ. Dietary nitrite supplementation protects against myocardial ischemia-reperfusion injury. *Proc Natl Acad Sci U S A* 104: 19144-9, 2007.
16. Buckley BJ, Li S, Whorton AR. Keap1 modification and nuclear accumulation in response to S-nitrosocysteine. *Free Radic Biol Med* 44: 692-8, 2008.
17. Buckley BJ, Marshall ZM, Whorton AR. Nitric oxide stimulates Nrf2 nuclear translocation in vascular endothelium. *Biochem Biophys Res Commun* 307: 973-9, 2003.
18. Cannon JR, Tapias V, Na HM, Honick AS, Drolet RE, Greenamyre JT. A highly reproducible rotenone model of Parkinson's disease. *Neurobiol Dis* 34: 279-90, 2009.
19. Chinta SJ, Andersen JK. Nitrosylation and nitration of mitochondrial complex I in Parkinson's disease. *Free Radic Res* 45: 53-8, 2011.
20. Chouchani ET, Methner C, Nadochiy SM, Logan A, Pell VR, Ding S, James AM, Cocheme HM, Reinhold J, Lilley KS, Partridge L, Fearnley IM, Robinson AJ, Hartley RC, Smith RA, Krieg T, Brookes PS, Murphy MP. Cardioprotection by S-nitrosation of a cysteine switch on mitochondrial complex I. *Nat Med* 19: 753-9, 2013.
21. Coert BA, Anderson RE, Meyer FB. A comparative study of the effects of two nitric oxide synthase inhibitors and two nitric oxide donors on temporary focal cerebral ischemia in the Wistar rat. *J Neurosurg* 90: 332-8, 1999.
22. Collier TJ, Kanaan NM, Kordower JH. Ageing as a primary risk factor for Parkinson's disease: evidence from studies of non-human primates. *Nat Rev Neurosci* 12: 359-66, 2011.

23. Cooper O, Seo H, Andrabi S, Guardia-Laguarta C, Graziotto J, Sundberg M, McLean JR, Carrillo-Reid L, Xie Z, Osborn T, Hargus G, Deleidi M, Lawson T, Bogetofte H, Perez-Torres E, Clark L, Moskowitz C, Mazzulli J, Chen L, Volpicelli-Daley L, Romero N, Jiang H, Uitti RJ, Huang Z, Opala G, Scarffe LA, Dawson VL, Klein C, Feng J, Ross OA, Trojanowski JQ, Lee VM, Marder K, Surmeier DJ, Wszolek ZK, Przedborski S, Krainc D, Dawson TM, Isacson O. Pharmacological rescue of mitochondrial deficits in iPSC-derived neural cells from patients with familial Parkinson's disease. *Sci Transl Med* 4: 141ra90, 2012.
24. Dhakshinamoorthy S, Porter AG. Nitric oxide-induced transcriptional up-regulation of protective genes by Nrf2 via the antioxidant response element counteracts apoptosis of neuroblastoma cells. *J Biol Chem* 279: 20096-107, 2004.
25. Dranka BP, Zielonka J, Kanthasamy AG, Kalyanaraman B. Alterations in bioenergetic function induced by Parkinson's disease mimetic compounds: lack of correlation with superoxide generation. *J Neurochem* 122: 941-51, 2012.
26. Drolet RE, Cannon JR, Montero L, Greenamyre JT. Chronic rotenone exposure reproduces Parkinson's disease gastrointestinal neuropathology. *Neurobiol Dis* 36: 96-102, 2009.
27. Duty S, Jenner P. Animal models of Parkinson's disease: a source of novel treatments and clues to the cause of the disease. *Br J Pharmacol* 164: 1357-91, 2011.
28. Fall CP, Bennett JP, Jr. Characterization and time course of MPP+ -induced apoptosis in human SH-SY5Y neuroblastoma cells. *J Neurosci Res* 55: 620-8, 1999.
29. Farrell TC, Cario CL, Milanese C, Vogt A, Jeong JH, Burton EA. Evaluation of spontaneous propulsive movement as a screening tool to detect rescue of Parkinsonism phenotypes in zebrafish models. *Neurobiol Dis* 44: 9-18, 2011.
30. Flinn L, Mortiboys H, Volkmann K, Koster RW, Ingham PW, Bandmann O. Complex I deficiency and dopaminergic neuronal cell loss in parkin-deficient zebrafish (*Danio rerio*). *Brain* 132: 1613-23, 2009.
31. Friederich JA, Butterworth JFt. Sodium nitroprusside: twenty years and counting. *Anesth Analg* 81: 152-62, 1995.
32. Giannopoulos S, Katsanos AH, Tsvigoulis G, Marshall RS. Statins and cerebral hemodynamics. *J Cereb Blood Flow Metab* 32: 1973-6, 2012.
33. Gladwin MT, Raat NJ, Shiva S, DeZfulian C, Hogg N, Kim-Shapiro DB, Patel RP. Nitrite as a vascular endocrine nitric oxide reservoir that contributes to hypoxic signaling, cytoprotection, and vasodilation. *Am J Physiol Heart Circ Physiol* 291: H2026-35, 2006.
34. Glinka Y, Tipton KF, Youdim MB. Nature of inhibition of mitochondrial respiratory complex I by 6-Hydroxydopamine. *J Neurochem* 66: 2004-10, 1996.
35. Glinka Y, Tipton KF, Youdim MB. Mechanism of inhibition of mitochondrial respiratory complex I by 6-hydroxydopamine and its prevention by desferrioxamine. *Eur J Pharmacol* 351: 121-9, 1998.
36. Hill BG, Dranka BP, Zou L, Chatham JC, Darley-Usmar VM. Importance of the bioenergetic reserve capacity in response to cardiomyocyte stress induced by 4-hydroxynonenal. *Biochem J* 424: 99-107, 2009.
37. Horowitz MP, Milanese C, Di Maio R, Hu X, Montero LM, Sanders LH, Tapias V, Sepe S, van Cappellen WA, Burton EA, Greenamyre JT, Mastroberardino PG. Single-cell redox imaging demonstrates a distinctive response of dopaminergic neurons to oxidative insults. *Antioxid Redox Signal* 15: 855-71, 2011.
38. Jazwa A, Rojo AI, Innamorato NG, Hesse M, Fernandez-Ruiz J, Cuadrado A. Pharmacological targeting of the transcription factor Nrf2 at the basal ganglia provides disease modifying therapy for experimental parkinsonism. *Antioxid Redox Signal* 14: 2347-60, 2011.
39. Kanga Pride C, Mo L, Quesnelle K, Dagda RK, Murillo D, Geary L, Corey C, Portella R, Zharikov S, St Croix C, Maniar S, Chu CT, Khoo NK, Shiva S. Nitrite activates protein kinase A in normoxia to mediate mitochondrial fusion and tolerance to ischaemia/reperfusion. *Cardiovasc Res* 101: 57-68, 2014.
40. Kaslin J, Panula P. Comparative anatomy of the histaminergic and other aminergic systems in zebrafish (*Danio rerio*). *J Comp Neurol* 440: 342-77, 2001.
41. Kordower JH, Olanow CW, Dodiya HB, Chu Y, Beach TG, Adler CH, Halliday GM, Bartus RT. Disease duration and the integrity of the nigrostriatal system in Parkinson's disease. *Brain* 136: 2419-31, 2013.
42. Kumari U, Tan EK. LRRK2 in Parkinson's disease: genetic and clinical studies from patients. *FEBS J* 276: 6455-63, 2009.
43. Larsen FJ, Schiffer TA, Borniquel S, Sahlin K, Ekblom B, Lundberg JO, Weitzberg E. Dietary inorganic nitrate improves mitochondrial efficiency in humans. *Cell Metab* 13: 149-59, 2011.
44. Lee YC, Lin CH, Wu RM, Lin MS, Lin JW, Chang CH, Lai MS. Discontinuation of statin therapy associates with Parkinson disease: a population-based study. *Neurology* 81: 410-6, 2013.

- 1
2
3 45. Lundberg JO, Gladwin MT, Weitzberg E. Strategies to increase nitric oxide signalling in cardiovascular
4 disease. *Nat Rev Drug Discov* 14: 623-41, 2015.
- 5 46. Lundberg JO, Weitzberg E, Gladwin MT. The nitrate-nitrite-nitric oxide pathway in physiology and
6 therapeutics. *Nat Rev Drug Discov* 7: 156-67, 2008.
- 7 47. Manzoni C, Mamais A, Dihanich S, McGoldrick P, Devine MJ, Zerle J, Kara E, Taanman JW, Healy DG,
8 Marti-Masso JF, Schapira AH, Plun-Favreau H, Tooze S, Hardy J, Bandopadhyay R, Lewis PA. Pathogenic
9 Parkinson's disease mutations across the functional domains of LRRK2 alter the autophagic/lysosomal response to
10 starvation. *Biochem Biophys Res Commun* 441: 862-6, 2013.
- 11 48. Mastroberardino PG, Orr AL, Hu X, Na HM, Greenamyre JT. A FRET-based method to study protein thiol
12 oxidation in histological preparations. *Free Radic Biol Med* 45: 971-81, 2008.
- 13 49. Mensinga TT, Speijers GJ, Meulenbelt J. Health implications of exposure to environmental nitrogenous
14 compounds. *Toxicol Rev* 22: 41-51, 2003.
- 15 50. Milanese C, Sager JJ, Bai Q, Farrell TC, Cannon JR, Greenamyre JT, Burton EA. Hypokinesia and reduced
16 dopamine levels in zebrafish lacking beta- and gamma1-synucleins. *J Biol Chem* 287: 2971-83, 2012.
- 17 51. Miller MR, Megson IL. Recent developments in nitric oxide donor drugs. *Br J Pharmacol* 151: 305-21,
18 2007.
- 19 52. Moncada S, Bolanos JP. Nitric oxide, cell bioenergetics and neurodegeneration. *J Neurochem* 97: 1676-89,
20 2006.
- 21 53. Motohashi H, Yamamoto M. Nrf2-Keap1 defines a physiologically important stress response mechanism.
22 *Trends Mol Med* 10: 549-57, 2004.
- 23 54. National Toxicology P. Toxicology and carcinogenesis studies of sodium nitrite (CAS NO. 7632-00-0) in
24 F344/N rats and B6C3F1 mice (drinking water studies). *Natl Toxicol Program Tech Rep Ser* 495: 7-273, 2001.
- 25 55. Niture SK, Khatri R, Jaiswal AK. Regulation of Nrf2-an update. *Free Radic Biol Med* 66: 36-44, 2014.
- 26 56. Panov A, Dikalov S, Shalbuyeva N, Taylor G, Sherer T, Greenamyre JT. Rotenone model of Parkinson
27 disease: multiple brain mitochondria dysfunctions after short term systemic rotenone intoxication. *J Biol Chem* 280:
28 42026-35, 2005.
- 29 57. Panula P, Sallinen V, Sundvik M, Kolehmainen J, Torkko V, Tiittula A, Moshnyakov M, Podlasz P.
30 Modulatory neurotransmitter systems and behavior: towards zebrafish models of neurodegenerative diseases.
31 *Zebrafish* 3: 235-47, 2006.
- 32 58. Paxinos G, Franklin KBJ. *The Mouse Brain in Stereotaxic Coordinates*: Elsevier Academic Press; 2004.
- 33 59. Przedborski S, Vila M. The 1-methyl-4-phenyl-1,2,3,6-tetrahydropyridine mouse model: a tool to explore
34 the pathogenesis of Parkinson's disease. *Ann N Y Acad Sci* 991: 189-98, 2003.
- 35 60. Raat NJ, Shiva S, Gladwin MT. Effects of nitrite on modulating ROS generation following ischemia and
36 reperfusion. *Adv Drug Deliv Rev* 61: 339-50, 2009.
- 37 61. Ramsay RR, Salach JJ, Singer TP. Uptake of the neurotoxin 1-methyl-4-phenylpyridine (MPP+) by
38 mitochondria and its relation to the inhibition of the mitochondrial oxidation of NAD+-linked substrates by MPP+.
39 *Biochem Biophys Res Commun* 134: 743-8, 1986.
- 40 62. Reddie KG, Carroll KS. Expanding the functional diversity of proteins through cysteine oxidation. *Curr*
41 *Opin Chem Biol* 12: 746-54, 2008.
- 42 63. Rink E, Wullmann MF. The teleostean (zebrafish) dopaminergic system ascending to the subpallium
43 (striatum) is located in the basal diencephalon (posterior tuberculum). *Brain Res* 889: 316-30, 2001.
- 44 64. Ryan SD, Dolatabadi N, Chan SF, Zhang X, Akhtar MW, Parker J, Soldner F, Sunico CR, Nagar S,
45 Talantova M, Lee B, Lopez K, Nutter A, Shan B, Molokanova E, Zhang Y, Han X, Nakamura T, Masliah E, Yates
46 JR, 3rd, Nakanishi N, Andreyev AY, Okamoto S, Jaenisch R, Ambasudhan R, Lipton SA. Isogenic human iPSC
47 Parkinson's model shows nitrosative stress-induced dysfunction in MEF2-PGC1alpha transcription. *Cell* 155: 1351-
48 64, 2013.
- 49 65. Sallinen V, Torkko V, Sundvik M, Reenila I, Khrustalyov D, Kaslin J, Panula P. MPTP and MPP+ target
50 specific aminergic cell populations in larval zebrafish. *J Neurochem* 108: 719-31, 2009.
- 51 66. Sherer TB, Betarbet R, Stout AK, Lund S, Baptista M, Panov AV, Cookson MR, Greenamyre JT. An in
52 vitro model of Parkinson's disease: linking mitochondrial impairment to altered alpha-synuclein metabolism and
53 oxidative damage. *J Neurosci* 22: 7006-15, 2002.
- 54 67. Shiva S, Sack MN, Greer JJ, Duranski M, Ringwood LA, Burwell L, Wang X, MacArthur PH, Shoja A,
55 Raghavachari N, Calvert JW, Brookes PS, Lefter DJ, Gladwin MT. Nitrite augments tolerance to
56 ischemia/reperfusion injury via the modulation of mitochondrial electron transfer. *J Exp Med* 204: 2089-102, 2007.
- 57 68. Tanner CM, Kamel F, Ross GW, Hoppin JA, Goldman SM, Korell M, Marras C, Bhudhikanok GS, Kasten
58 M, Chade AR, Comyns K, Richards MB, Meng C, Priestley B, Fernandez HH, Cambi F, Umbach DM, Blair A,
59
60

- 1
2
3 Sandler DP, Langston JW. Rotenone, paraquat, and Parkinson's disease. *Environ Health Perspect* 119: 866-72,
4 2011.
- 5 69. Tanner CM, Ross GW, Jewell SA, Hauser RA, Jankovic J, Factor SA, Bressman S, Deligtisch A, Marras C,
6 Lyons KE, Bhudhikanok GS, Roucoux DF, Meng C, Abbott RD, Langston JW. Occupation and risk of
7 parkinsonism: a multicenter case-control study. *Arch Neurol* 66: 1106-13, 2009.
- 8 70. Tapias V, Cannon JR, Greenamyre JT. Pomegranate juice exacerbates oxidative stress and nigrostriatal
9 degeneration in Parkinson's disease. *Neurobiol Aging* 35: 1162-76, 2014.
- 10 71. Tapias V, Greenamyre JT, Watkins SC. Automated imaging system for fast quantitation of neurons, cell
11 morphology and neurite morphometry in vivo and in vitro. *Neurobiol Dis* 54: 158-68, 2013.
- 12 72. Um HC, Jang JH, Kim DH, Lee C, Surh YJ. Nitric oxide activates Nrf2 through S-nitrosylation of Keap1 in
13 PC12 cells. *Nitric Oxide* 25: 161-8, 2011.
- 14 73. Wang X, Kettenhofen NJ, Shiva S, Hogg N, Gladwin MT. Copper dependence of the biotin switch assay:
15 modified assay for measuring cellular and blood nitrosated proteins. *Free Radic Biol Med* 44: 1362-72, 2008.
- 16 74. West MJ, Gundersen HJ. Unbiased stereological estimation of the number of neurons in the human
17 hippocampus. *J Comp Neurol* 296: 1-22, 1990.
- 18
19
20
21
22
23
24
25
26
27
28
29
30
31
32
33
34
35
36
37
38
39
40
41
42
43
44
45
46
47
48
49
50
51
52
53
54
55
56
57
58
59
60

Tables

Table 1: PD patients' and controls' related information

Description	Gender	Age	Race	Affected	Gene	Mutation
ND32975	Female	74	Caucasian	Yes	LRRK2	ARG1441GLY
ND32976	Female	69	Caucasian	Yes	LRRK2	ARG1441GLY
ND33879	Female	66	Caucasian	Yes	LRRK2	GLY2019SER
AG08269	Female	82	Caucasian	no	no	no
CHDF	Male	62	Caucasian	no	no	no

Table 2: Primers list

Description	Gene	Forward (5'-3')	Reverse
Tyrosine 3-monooxygenase/tryptophan 5-monooxygenase activation protein, zeta polypeptide	YWHAZ	CCTGCATGAAGTCTGTAAGTCTGAG	GACCTACGGGCTCCTACAACA
Ribosomal protein, large, P0	RPLP0	AGCCCAGAACACTGGTCTC	ACTCAGGATTTCAATGGTGCC
Catalase	CAT	AGATGCAGCACTGGAAGGA	CACGGGGCCCTACTGTAATA
Glutamate-cysteine ligase, catalytic subunit	GCLC	AGGACGTTCTCAAGTGGGG	GTCCTTTCCCTTCTCTTG

Figure legends

Fig.1. Nitrite ameliorates MPP⁺ effects on TH-immunoreactive neurons in zebrafish larvae.

(A) Schematic of the experimental design: one day post-fertilization embryos were treated with nitrite dissolved in E3 water for 4 days. The compound was then removed and the larvae were exposed for 48 hours to 1 mM MPP⁺. (B). Sagittal overview of the zebrafish brain showing the localization of the *posterior tuberculum* (PT). Ob: *Olfactory bulb*; Tel: *Telencephalon*; TeO: *Tectum Opticum*; CCe: *Corpus Cerebelli*; Mo: *Medulla oblongata*; MS: *Medulla spinalis*; TH: *Tuberal hypothalamus*; Hyp: *Hypothalamus*. (C) Exposure to MPP⁺ reduces the number of TH-positive neurons in the posterior tuberculum (PT); 4 days nitrite pretreatment (1 and 10 μM) significantly prevents neuronal cell loss. (D-M) Representative images of a sagittal overview of TH positive neuronal clusters distribution in 7 dpf zebrafish larvae brains exposed to nitrite (H-M) and MPP⁺ (F-M) treatments. The catecholaminergic clusters in the PT are magnified in the insets (E, G, I, M). Scale bars: 50 μm. (N-P) Spontaneous motor activity of 7 dpf zebrafish larvae exposed to nitrite and/or MPP⁺. (N) Representative image of the characteristic swimming pattern of larvae in a single-larva/single-well set up after treatments. Activity is expressed in terms of mean velocity (O) and percentage of time spent moving (P) in a 2 hours-recording time frame. Results shown in b are based on two independent technical replicates and results shown in N-O represent four independent technical replicates (*p < 0.05; ** p < 0.01; *** p < 0.001; one way ANOVA followed by Dunnett's multiple comparison *post doc* test). Graphs represent mean ± s.e.m. (To see this illustration in color the reader is referred to the web version of this article at www.liebertonline.com/ars).

1
2
3 **Fig. 2. Nitrite administration ameliorates pathology in rotenone and 6-OHDA rat models**
4 **of PD.**
5

6
7 (A) Schematic of the experimental paradigm for nitrite and rotenone administration. (B).
8 Representative image of striatal TH immunohistochemistry reveals severe depletion in DA fibers
9 following rotenone exposure, which is strongly mitigated upon treatment with inorganic nitrite
10 (scale bar: 1mm). (C) Representative image of rotenone induced DA loss in the SNpc, which is
11 prevented by nitrite co-treatment (scale bar: 100µm). (D) Quantification of striatal innervation in
12 (B) by densitometry. (E) Quantification of DA loss in the SNpc (C) by unbiased stereological
13 counts. (F) Experimental 6-OHDA set-up: in the *acute paradigm* (top) nitrite was administered
14 24- and 1- hour before stereotactic infusion in the rat striatum; in the *chronic paradigm* (bottom),
15 nitrite was administered orally, dissolved in drinking water, starting 7 days after induction of the
16 lesion. (G, H) Nitrite administration ameliorates the 6-OHDA induced lesions in striata and in
17 *substantia nigra pars compacta*. (I) Representative images of striata cross-sections injected with
18 6-OHDA (*Ipsilateral*) and the respective untreated side (*Contralateral*) of nitrite-treated rats.
19 (Scale bar: 1mm). (*p < 0.05; **p < 0.01; one way ANOVA followed by Dunnett's multiple
20 comparison *post doc* test for D, E, G; two sided Student's t-test for H). Graph represents mean
21 ± s.e.m. (To see this illustration in color the reader is referred to the web version of this article at
22 www.liebertonline.com/ars).
23
24
25
26
27
28
29
30
31
32
33
34
35
36
37
38
39
40
41
42
43
44
45
46
47
48
49
50
51
52
53
54
55
56
57
58
59
60

1
2
3 **Fig. 3. Nitrite improves mitochondrial respiration in dermal fibroblasts from PD patients**
4 **harboring LRRK2 mutations.**
5

6
7
8 (A) Oxygen consumption rate (OCR) profile of fibroblast from healthy subjects pre-treated 48
9 hours with nitrite (1 or 10 μ M). Fibroblasts were challenged with sequential administration of
10 oligomycin to inhibit ATP synthase, FCCP to elicit maximal respiration, rotenone to inhibit
11 complex I, and antimycin to inhibit complex III and fully block respiration. The parameters
12 analyzed in the profile were: basal respiration, proton leakage, mitochondrial reserve capacity
13 (as difference between maximum reserve capacity and basal respiration) and rotenone sensitive
14 respiration, which accounts for the respiration dependent on complex I. (B-D) Quantification of
15 basal OCR levels (B), rotenone sensitive respiration (C) and reserve capacity (D) of fibroblasts
16 derived from healthy controls and LRRK2-PD patients. (E-G) Administration of nitrite
17 significantly improves mitochondrial respiration in PD fibroblast by decreasing proton leakage
18 (E), increasing the rotenone sensitive respiration (F), and reserve capacity (G). OCR values
19 are expressed as % of variation from the baseline. Results are based on 3 independent
20 experiments. (* $p < 0.05$; ** $p < 0.01$; *** $p < 0.001$; one way ANOVA followed by Dunnett's
21 multiple comparison *post doc* test). Graphs represent mean \pm s.e.m.
22
23
24
25
26
27
28
29
30
31
32
33
34
35
36
37
38
39
40
41
42
43
44
45
46
47
48
49
50
51
52
53
54
55
56
57
58
59
60

Fig. 4. Mechanisms underlying nitrite cytoprotection.

(A). Experimental design; after 48 hours of incubation, nitrite was removed from the medium and SH-SY5Y cells were exposed to MPP⁺. (B, C) Effects of nitrite pre-treatment on MPP⁺ cytotoxicity (100 μM in B and 5 mM in C); nitrite administration significantly reduces cell death.

(D) Representative image of the in-gel detection of protein S-nitrosation (SNO) following MPP⁺ (100 μM) and/or nitrite treatment. Free cysteine-thiols were blocked with NEM and S-nitrosated cysteines were labeled with fluorescent NEM following reduction with ascorbate and Cu⁺⁺ (SNO, green signal). As a loading control, total proteins were labeled with NHS-ester (red signal).

(E) While MPP⁺ exposure does not induce changes in protein S-nitrosation, pretreatment with nitrite significantly increases SNO levels. (F, G) H₂O₂ induces rapid formation of sulfenic acid on cysteines, which is prevented by nitrite mediated S-nitrosation pre-treatment. SH-SY5Y cells were treated with 0.5 mM H₂O₂ and lysed in presence of dimedone. Nitrite pre-treated samples showed reduced formation of dimedone adducts (arrowheads in F – representative image). The bar graph (G) represents densitometric analysis of the whole lane normalized over actin.

(H) Superoxide production in SH-SY5Y exposed to 4 hours of 100 μM MPP⁺. Nitrite pretreatment does not prevent the increase in superoxide production induced by MPP⁺ exposure. Results are based on 3 independent experiments. (*p < 0.05; **p < 0.01; ***p < 0.001; one way ANOVA followed by Dunnett's multiple comparison *post doc* test). Graphs represent mean ± s.e.m. (To see this illustration in color the reader is referred to the web version of this article at www.liebertonline.com/ars).

1
2
3 **Fig. 5. Nitrite pretreatment improves the recovery of mitochondrial respiration and**
4 **induces Keap1 S-nitrosation.**
5
6

7
8 (A) Nitrite administration stimulates recovery of mitochondrial respiration after a transient 4
9 hours exposure to MPP⁺. SH-SY5Y cells were seeded in a Seahorse Bioscience V7 tissue
10 Culture plate, incubated with nitrite for 48 hours, and then treated with 100 μ M MPP⁺. After 4
11 hours, MPP⁺ was removed and basal oxygen consumption rate (OCR) was monitored for 8
12 hours with a Seahorse XF24 Extracellular Flow Analyzer. Nitrite pretreated cells reached control
13 OCR levels after 76 (10 μ M, gray arrowhead) and 130 (1 μ M, black arrowhead) minutes, while
14 respiration in cells treated only with MPP⁺ remain consistently lower than controls. (B)
15 Representative in gel detection of S-nitrosated (SNO, left panel) and reduced (SH, central
16 panel) cysteine thiols in immunocaptured mitochondrial complex I extracted from cells treated
17 with nitrite and/or MPP⁺ reveals reduction of mitochondrial complex I protein cysteines in MPP⁺
18 specimen pretreated with nitrite (compare lane 7 with other lanes). Gel protein loading was
19 assessed by silver staining (right panel). (C, D) Nitrate administration induces S-nitrosation of
20 Keap1. SH-SY5Y cells received a 48 hours treatment with nitrite (1 or 10 μ M) or a 30' treatment
21 with H₂O₂ (0.5mM), and the biotin switch reaction was performed in all samples in presence of
22 biotin-NEM, Cu⁺⁺ and ascorbate. Biotinylated proteins were captured with streptavidin-
23 conjugated beads, separated on a gel and probed with an anti-Keap1 antibody (C,
24 representative image, full gel in supplementary figure 2). S-nitrosated-Keap1 levels were
25 normalized on the pre-captured SNO-modified total lysates labeled with NHS-ester (D). **p <
26 0.01; one way ANOVA followed by Dunnett's multiple comparison *post doc* test. Graphs
27 represent mean \pm s.e.m.
28
29
30
31
32
33
34
35
36
37
38
39
40
41
42
43
44
45
46
47
48
49
50
51
52
53
54
55
56
57
58
59
60

1
2
3 **Fig. 6. Nitrite pretreatment promotes the activation of the antioxidant response via**
4 **nuclear translocation of the Nrf2 transcription factor.**
5
6

7
8 (A) Transient GFP-Nrf2 expression in SH-SH5Y cells 24 hours (line 1) and 48 hours (line 2)
9 after transfection. Empty GFP vector expression was used as control (line 3, 48 hours after
10 transfection), (B, C) Nuclear localization of GFP-Nrf2 (B) and GFP (C) after nitrite and MPP⁺
11 treatments in SH-SY5Y transfected cells. (D) A representative image showing that nitrite pre-
12 treatment promotes GFP-Nrf2 translocation to the nucleus (Scale bar: 20 μm). (E) Nitrite-
13 induced Nrf2 mobilization to the nucleus; translocation is exacerbated by MPP⁺ treatment. (F)
14 Nrf2 translocation requires bioavailability of NO because it is repressed by the NO scavenger
15 Carboxy-PTIO. (G) Nuclear translocation is inhibited by treatment with the Nrf2 inhibitor
16 trigonelline. (H, I) Nrf2 nuclear translocation is associated with increased expression of Nrf2
17 target genes. (L) Graphical representation modeling the temporal sequence of protein
18 nitrosation (green), Nrf2 activation (blue), and cysteine reduction (red) following nitrite and/or
19 MPP⁺ administration. (*p < 0.05; **p < 0.01; ***p < 0.001; one way ANOVA followed by
20 Dunnett's multiple comparison *post doc* test). Graphs represent mean ± s.e.m. (To see this
21 illustration in color the reader is referred to the web version of this article at
22 www.liebertonline.com/ars).
23
24
25
26
27
28
29
30
31
32
33
34
35
36
37
38
39
40
41
42
43
44
45
46
47
48
49
50
51
52
53
54
55
56
57
58
59
60

Supplementary figure 1

(A) Representative image of the in-gel detection of protein S-nitrosation (SNO) following nitrite (1 or 10 μ M) treatment. SNO modified cysteines were labeled with fluorescent NEM following reduction with ascorbate and Cu^{++} (SNO, green signal). As a loading control, total proteins were labeled with NHS-ester (red signal). (B) Pretreatment with nitrite significantly increases SNO levels.

1
2
3
4
5
6
7
8
9
10
11
12
13
14
15
16
17
18
19
20
21
22
23
24
25
26
27
28
29
30
31
32
33
34
35
36
37
38
39
40
41
42
43
44
45
46
47
48
49
50
51
52
53
54
55
56
57
58
59
60

Supplementary figure 2

Original full size western blot showed in figure 5C. Anti-Keap1 antibody was used to detect Keap1 after the biotin switch reaction and the streptavidin SNO-biotin protein capture.

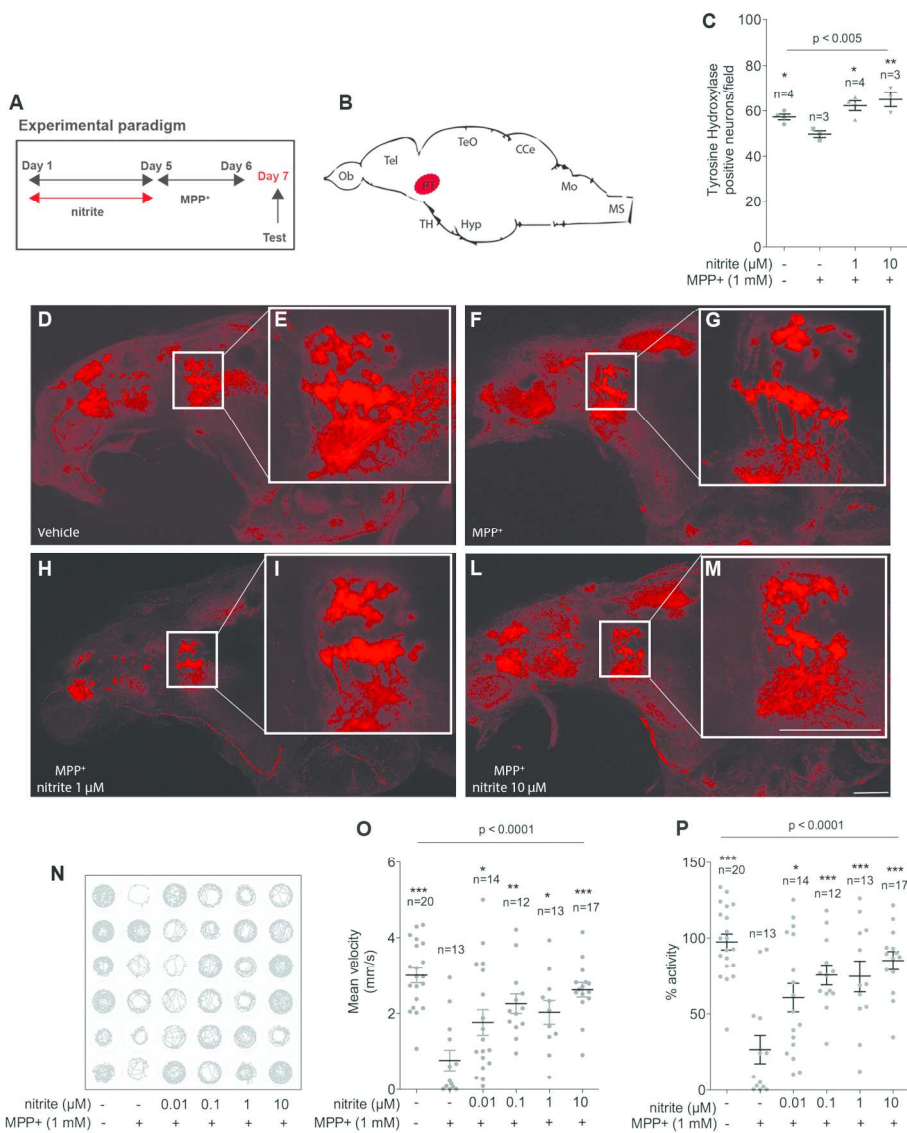
CONFIDENTIAL - For Peer Review Only

Supplementary figure 3

(A) Representative image showing that nitrite pre-treatment promotes Nfr2 translocation to the nucleus. The treatment with MPP⁺ exacerbates the migration to the nucleus (Scale bar: 20 μ m).

Supplementary figure 4

(A-D) S-nitrosation levels of mitochondrial proteins in organelles extracted from the ventral mesencephalic region of rodents injected with nitrite or vehicle (PBS). Fresh mitochondria were extracted from the ventral midbrain area 3 (A) or 7 (B) days after the injection and the biotin switch reaction was performed on mitochondrial lysates with fluorescent NEM in the presence of Cu^{++} and ascorbate (A, B). Reaction products were separated on a SDS protein gel and the signal intensity was quantified. NHS ester was used for loading normalization and relative densitometric quantification (C, D). (E-F) Immunodetection of the mitochondrial complex I protein Ndufa9 in mitochondrial protein extracts. S-Nitrosation was specifically detected with fluorescent maleimide and its levels are shown in right side panel; the same membrane was subsequently probed with an antibody against the mitochondrial complex I protein Ndufa9, which was then revealed by enhanced chemiluminescence (left). Quantitative evaluation of S-nitrosation levels normalized by the expression levels of Ndufa9 is represented in the graph (F).



Nitrite ameliorates MPP+ effects on TH-immunoreactive neurons in zebrafish larvae.

144x184mm (300 x 300 DPI)

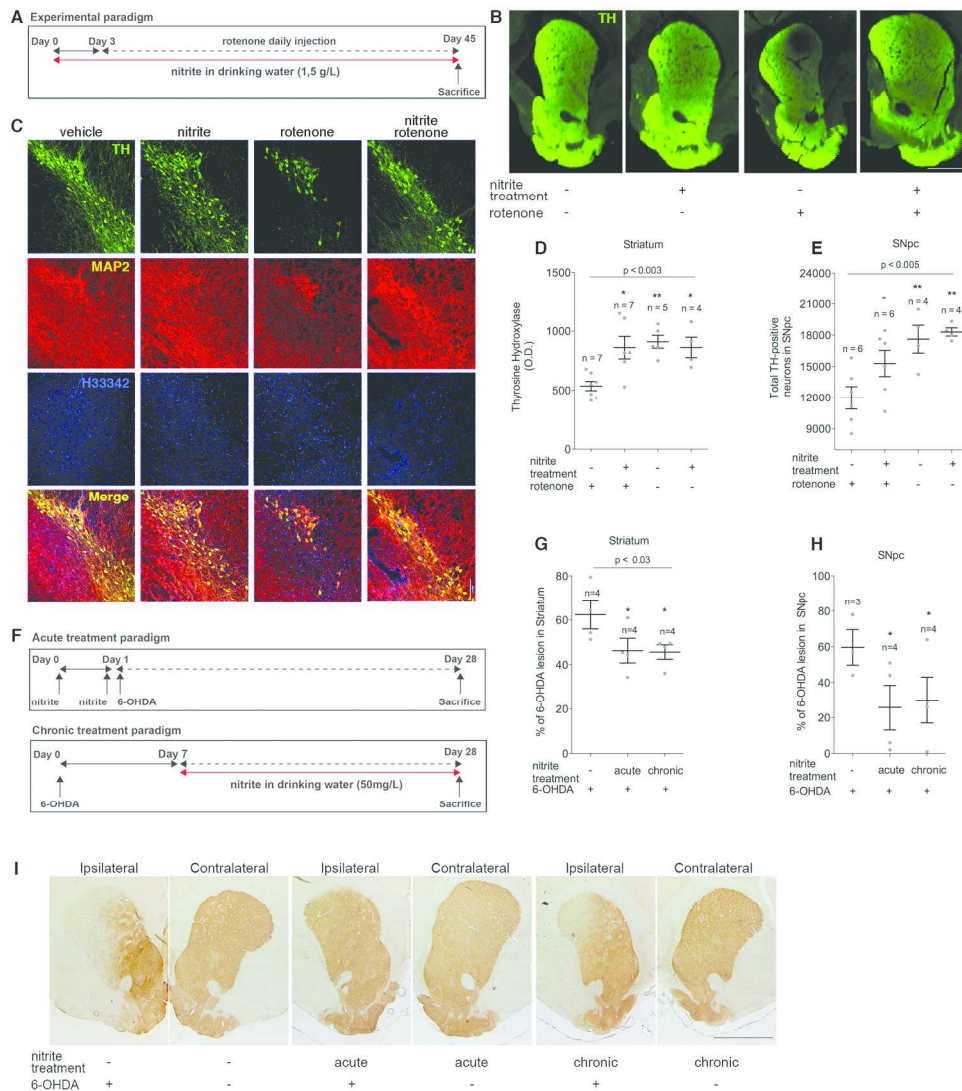


Fig. 2. Nitrite administration ameliorates pathology in rotenone and 6-OHDA rat models of PD.

180x199mm (300 x 300 DPI)

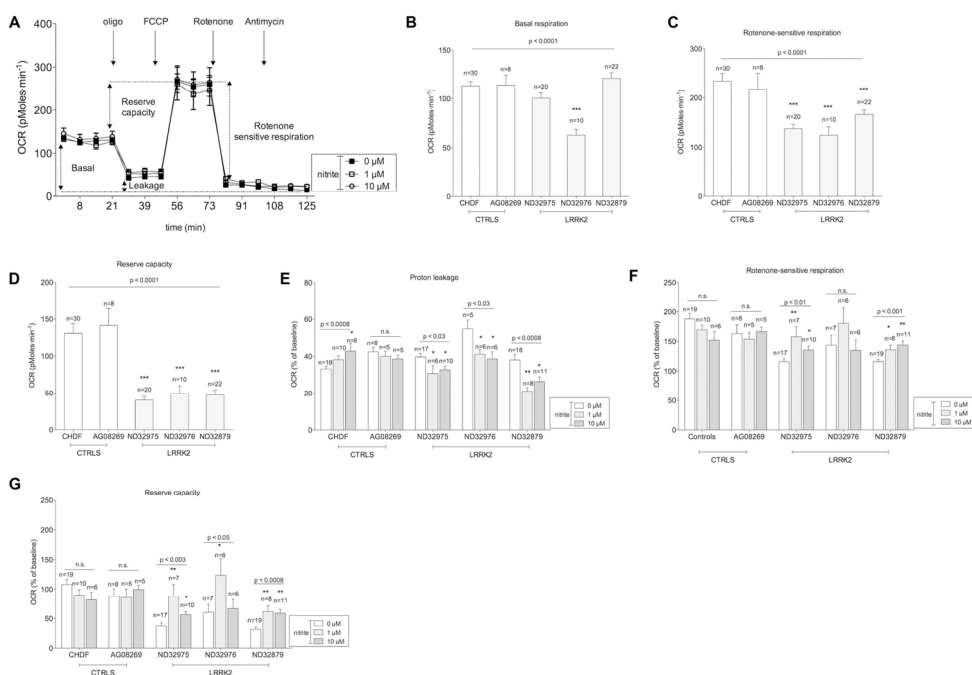


Fig. 3. Nitrite improves mitochondrial respiration in dermal fibroblasts from PD patients harboring LRRK2 mutations.

141x100mm (300 x 300 DPI)

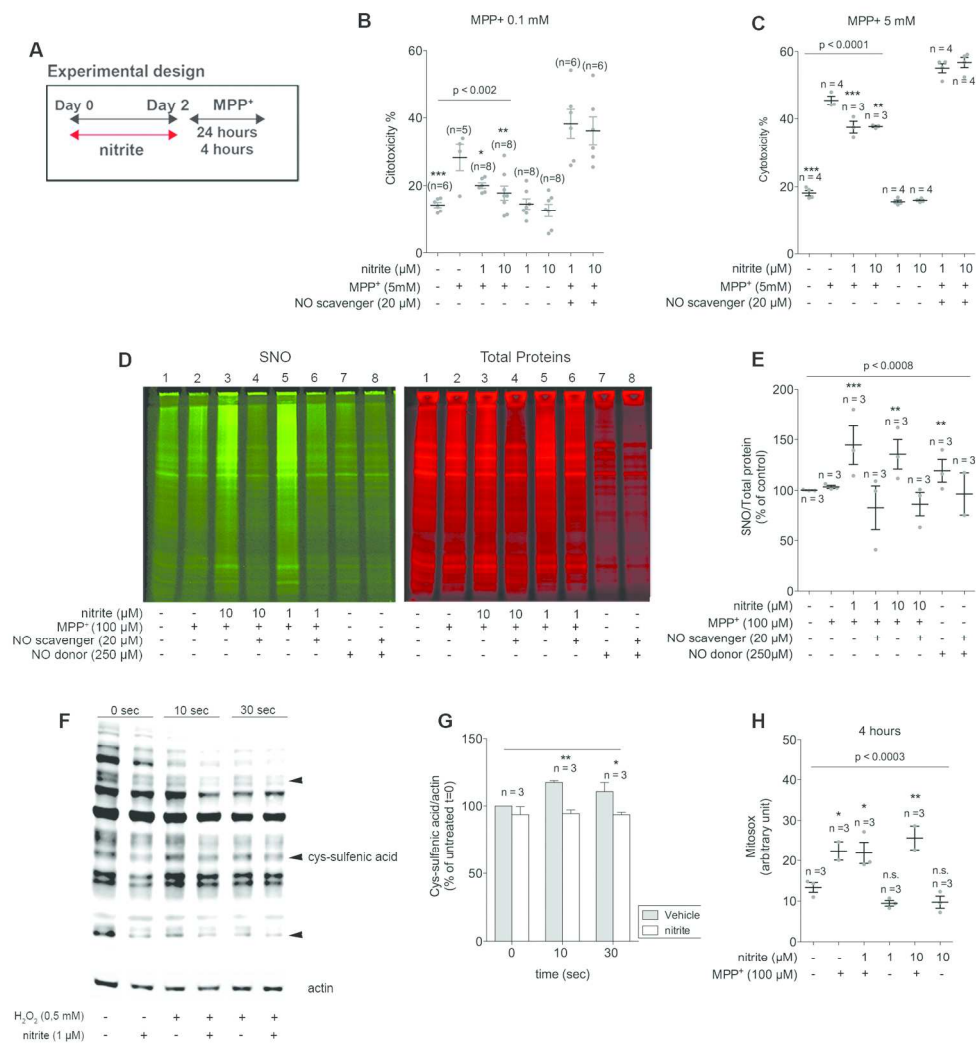


Fig. 4. Mechanisms underlying nitrite cytoprotection.

158x168mm (300 x 300 DPI)

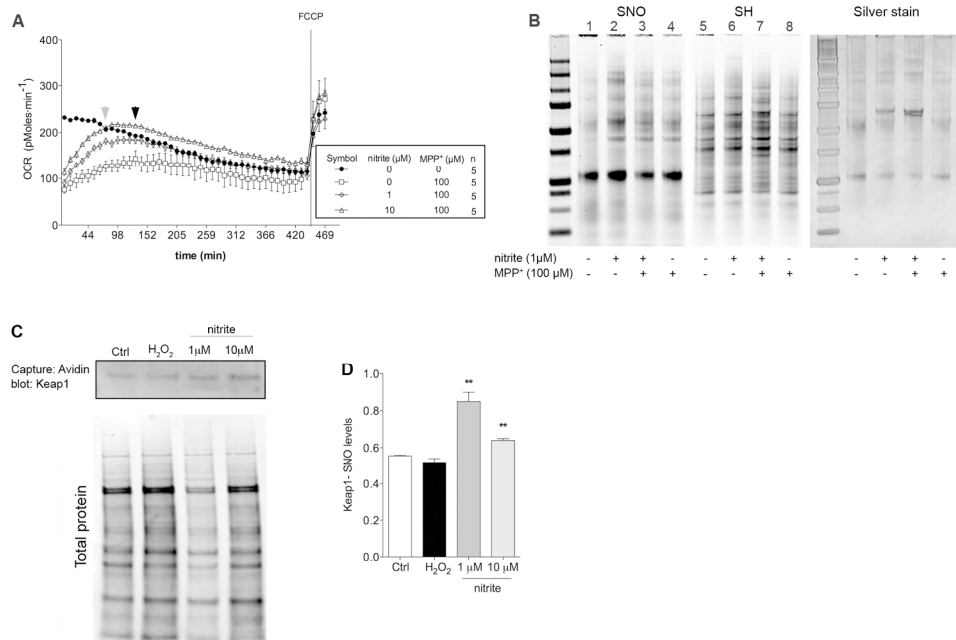


Fig. 5. Nitrite pretreatment improves the recovery of mitochondrial respiration and induces Keap1 S-nitrosylation.

183x126mm (300 x 300 DPI)

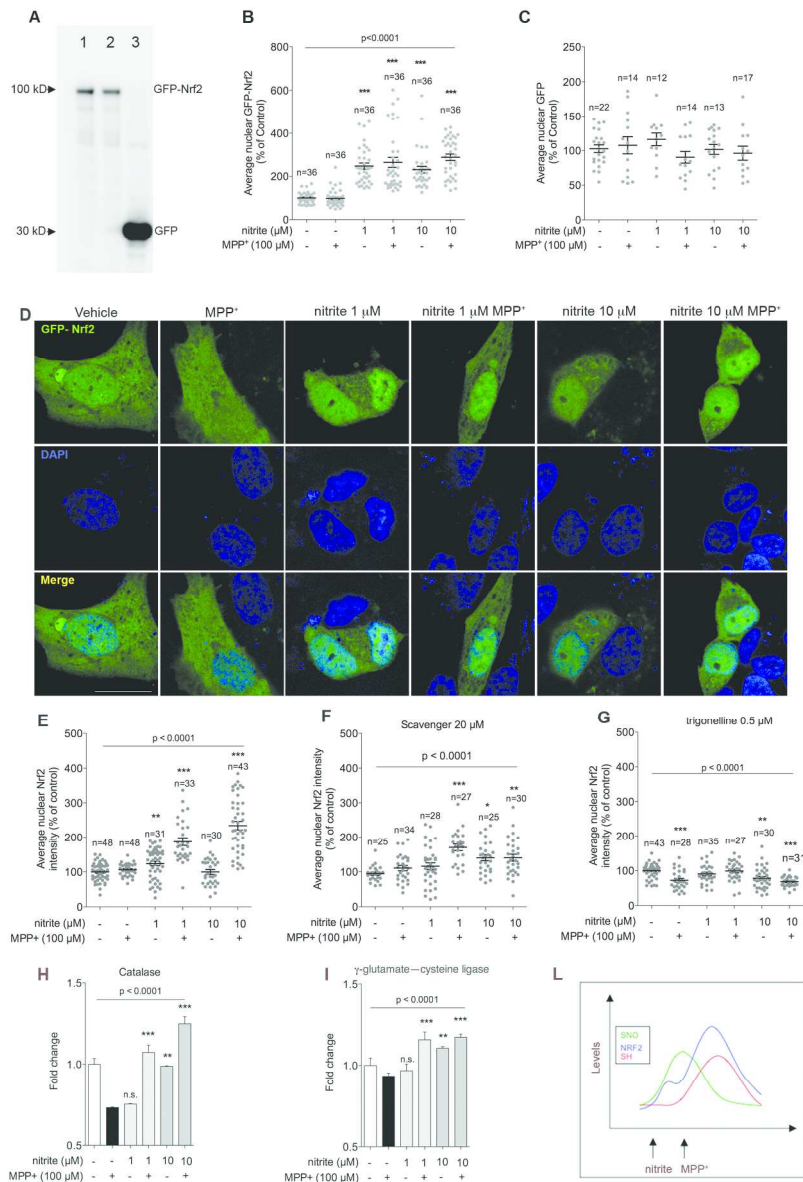
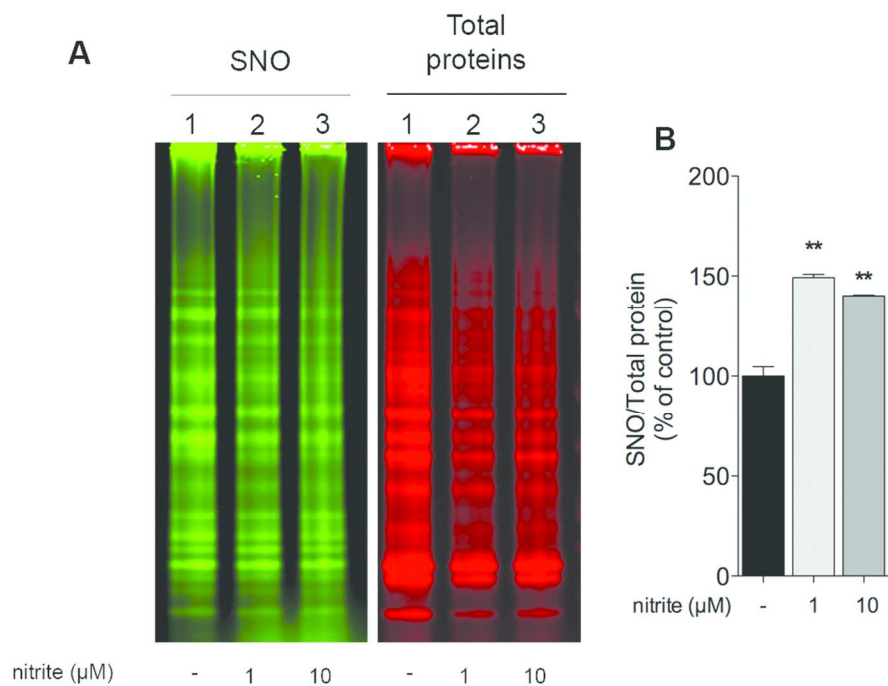


Fig. 6. Nitrite pretreatment promotes the activation of the antioxidant response via nuclear translocation of the Nrf2 transcription factor.

151x222mm (300 x 300 DPI)

Supplementary figure 1

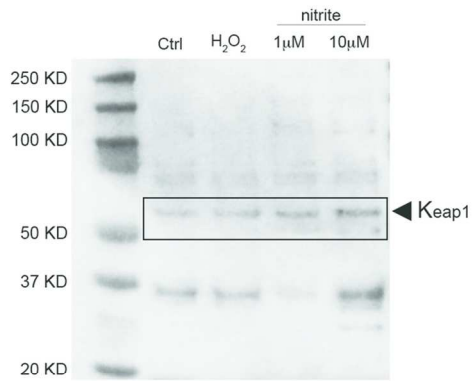


Supplementary figure 1

99x84mm (300 x 300 DPI)

1
2
3
4
5
6
7
8
9
10
11
12
13
14
15
16
17
18
19
20
21
22
23
24
25
26
27
28
29
30
31
32
33
34
35
36
37
38
39
40
41
42
43
44
45
46
47
48
49
50
51
52
53
54
55
56
57
58
59
60

Supplementary Figure 2

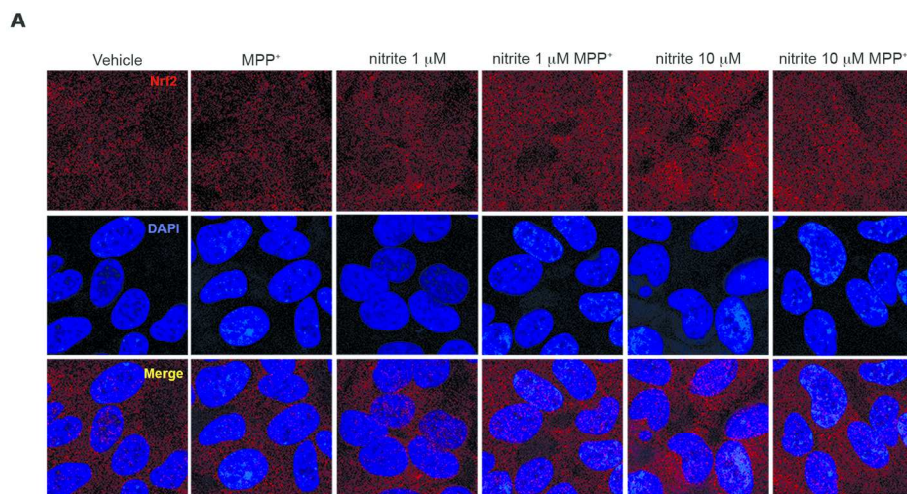


Supplementary figure 2

115x107mm (300 x 300 DPI)

Review Only

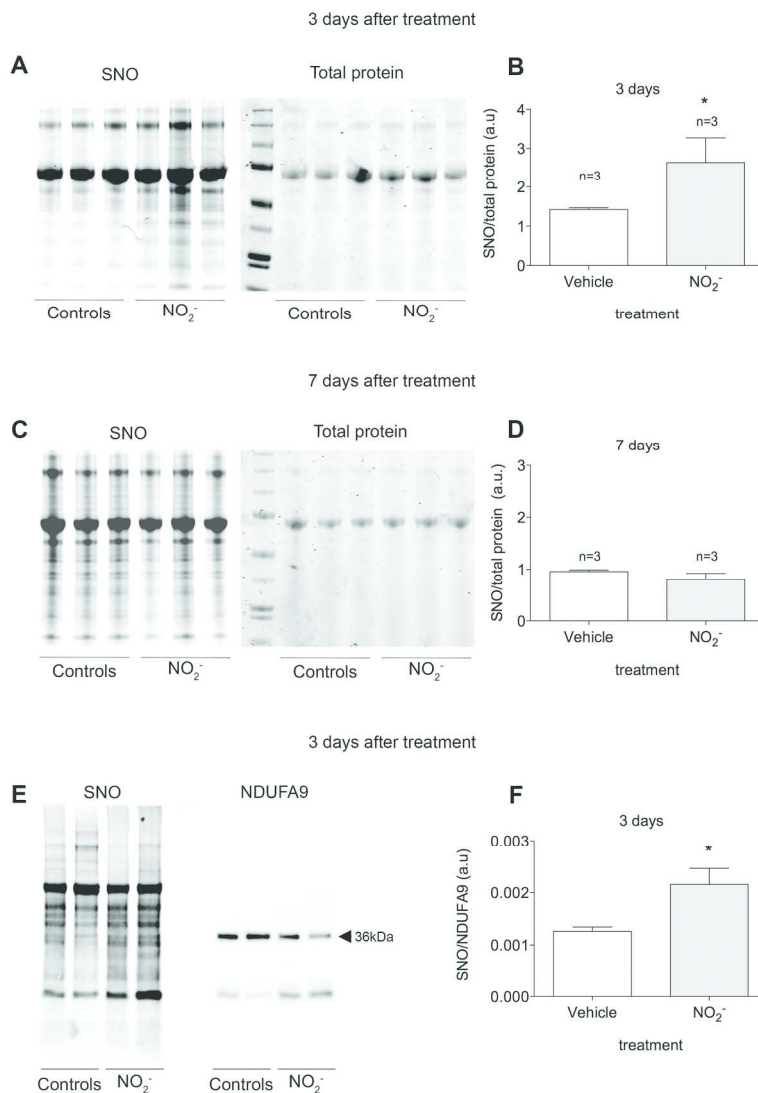
Supplementary figure 3



Supplementary figure 3

159x98mm (300 x 300 DPI)

Supplementary figure 4



Supplementary figure 4

156x233mm (300 x 300 DPI)